Theory of Parcel Vorticity Evolution in Supercell-Like Flows

ROBERT DAVIES-JONES[a]

[a] *NOAA/National Severe Storms Laboratory, Norman, Oklahoma*

(Manuscript received 2 July 2021, in final form 17 January 2022)

ABSTRACT: In a prior paper, insights into tornadogenesis in supercell storms were gained by discovering analytical formulas for vorticity variations along streamlines in idealized, steady, frictionless, isentropic inflows of dry air imported from a horizontally uniform environment. This work is simplified and extended to the evolution of parcel vorticity in unsteady, nonisentropic flows by integrating the vorticity equation using nonorthogonal Lagrangian coordinates. The covariant basis vectors $\bar{\mathbf{e}}_1$, $\bar{\mathbf{e}}_2$, and $\bar{\mathbf{e}}_3$ are material line elements attached to each parcel. Initially they form an orthonormal set with $\bar{\mathbf{e}}_1$ in the direction of and $\bar{\mathbf{e}}_2$ left normal to the storm-relative wind at each level in the environment, and $\bar{\mathbf{e}}_3$ upward. The surface containing all parcels with the same initial height constitutes a material surface, within which initially streamwise and transverse material lines are reoriented and stretched or shrunk. The basis vectors propagate a parcel's barotropic vorticity through time by factoring in the "frozen-field" effect. With a horizontally uniform environment, the barotropic vorticity of a parcel depends on its initial streamwise vorticity times its current $\bar{\mathbf{e}}_1$ plus its initial crosswise vorticity times its current $\bar{\mathbf{e}}_2$. For baroclinic and frictional vorticity, each contravariant component is the integral from initial to current time of the corresponding contravariant component of the generation vector. The "river-bend" effect acting on all parts (baroclinic, frictional, and barotropic) of transverse vorticity produces streamwise vorticity (parallel to 3D wind). In left-turning steady flow, it arises from $\bar{\mathbf{e}}_2$ rotating toward $\bar{\mathbf{e}}_1$. For steady, frictionless, dry isentropic flow, previous vorticity formulas are recovered.

SIGNIFICANCE STATEMENT: Air parcels rising in a tornado spin rapidly about their direction of motion. Theory herein describes the processes that can produce this streamwise spin in supercells. Cyclonic updraft rotation originates from strong low-level environmental storm-relative winds that turn clockwise with height. Parcels flowing into the updraft have initially large streamwise spins that are amplified by streamwise stretching. Rain curtains falling through the cyclonic updraft cause other parcels to descend and turn leftward. Buoyancy and frictional torques give them horizontal spin. Even if these spins are transverse to the flow initially, they are turned streamwise by secondary flow that develops in left-hand bends. As the parcels reach the ground and converge into the tornado, streamwise stretching greatly magnifies their streamwise spins.

KEYWORDS: Tornadogenesis; Mesocyclones; Supercells; Vorticity

1. Introduction

Three-dimensional high-resolution numerical simulations of supercell storms are now capable of reproducing violent tornadoes (e.g., Orf et al. 2017; Orf 2019). Despite excellent visualizations and extensive diagnostic studies of these complex simulations, there is still no universally accepted explanation of how the tornadoes form. This paper develops formulas for the partial vorticities of parcels that can be used to detect the origins of tornado vorticity in supercell simulations and thus assess the merits of various tornado theories. A subsequent paper will report and lightly test a methodology for computing partial vorticities of a parcel along its forward trajectory. The method requires the parcel's initial vorticity and, along its path, its velocity-gradient matrix and the torques acting on it. This information can be obtained from the output of a simulation.

Davies-Jones: Emeritus.

Corresponding author: Robert Davies-Jones, bobdj1066@yahoo.com

Although still not providing conclusive evidence in favor of a single tornadogenesis theory, numerical simulations have nevertheless provided clues. The following briefly summarizes current knowledge and ideas about tornado formation. In the typical supercell environment, vertical vorticity is negligible compared to horizontal vorticity (Davies-Jones 1984, hereafter DJ84). Moreover, simulated supercells produce tornadoes even when there is no environmental vertical vorticity. Thus Earth's rotation is essential only to the establishment of the favorable environmental wind shear that is input to a forecast or model. Within a storm, torques associated with differential buoyancy, frictional, and precipitation-drag forces generate vorticity that is predominantly horizontal. Thus any tornadogenesis theory should explain how the larger-scale flow in a simulated supercell can produce a tornado with its large vertical vorticity and high energy density at ground level from ambient and torque-generated horizontal vorticity. In theory and many simulations with a free-slip lower boundary condition, intense vertical vorticity near the ground forms from horizontal vorticity only in air parcels that have descended from their initial height in the environment (Davies-Jones 1982, 2000; Davies-Jones and Brooks 1993; Adlerman et al. 1999; Davies-Jones et al. 2001; Davies-Jones and Markowski

DOI: 10.1175/JAS-D-21-0178.1

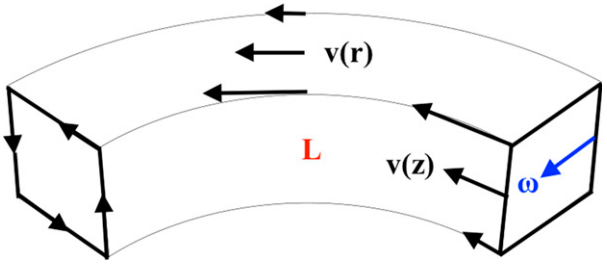

FIG. 1. 3D diagram of streamwise-vorticity development around a left-hand bend (thin black lines). Black arrows on the inner bank of the bend entrance indicate the vertical profile $\mathbf{v}(z)$ of the primary flow, which has positive speed shear. The blue arrow indicates the direction of the primary transverse vorticity entering the bend. The black arrows on the top face depict the lateral profile in downstream velocity, denoted by $\mathbf{v}(r)$, where r is distance from the bend's center of curvature. The red "L" indicates low pressure on the inside of the bend. High pressure on the outside of the bend is not shown. The black arrows at the exit of the bend indicate the sense of the secondary transverse circulation produced in the bend (adapted from Davies-Jones and Markowski 2021).

2013). As shown by Davies-Jones (2017, hereafter DJ17) and Rotunno et al. (2017), a current of air entering a tornado has to subside first in order for its horizontal vorticity to be greatly amplified next to the ground. The vortex then results from upward tilting of the crowded near-surface vortex lines. The near-ground vertical vorticity in many simulations stems from baroclinically generated horizontal vorticity in cool subsiding air on the left side of the storm with respect to storm motion (e.g., Rotunno and Klemp 1985; Davies-Jones and Brooks 1993; Adlerman et al. 1999; Dahl et al. 2014; Markowski and Richardson 2014; Dahl 2015). Even when the environmental vorticity is mainly crosswise (left normal to the storm-relative environmental wind) or when the baroclinic generation is transverse, the vorticity entering the tornadic region of the storm can still end up predominantly streamwise (Adlerman et al. 1999; Markowski and Richardson 2014) owing to the "river-bend effect," which turns positive transverse vorticity into the streamwise direction in left-turning flow (Fig. 1; Shapiro 1972; Scorer 1997; Adlerman et al. 1999; Davies-Jones et al. 2001; DJ17).

Recently other origins of vorticity have been proposed. In supercell simulations with surface drag, substantial increases in circulation around a material circuit have been attributed to frictionally generated vorticity generated close to the ground in the storm inflow (e.g., Roberts et al. 2020). Vorticity generated at the ground diffuses into the atmosphere. Owing to large vertical gradients of shear stress, the generation of frictional vorticity near the ground is predominantly horizontal. Like subsidence, surface drag causes packed near-surface vortex lines. Turbulent mixing in the model should be sufficient to produce a realistic surface layer. If this layer is too shallow, the frictional vorticity is too concentrated near the ground (Markowski and Bryan 2016; Davies-Jones 2021). However, Batchelor (1967, p. 282) pointed out that downward advection can confine vorticity to a shallow layer. Tornado formation could result if this abundant vorticity is advected

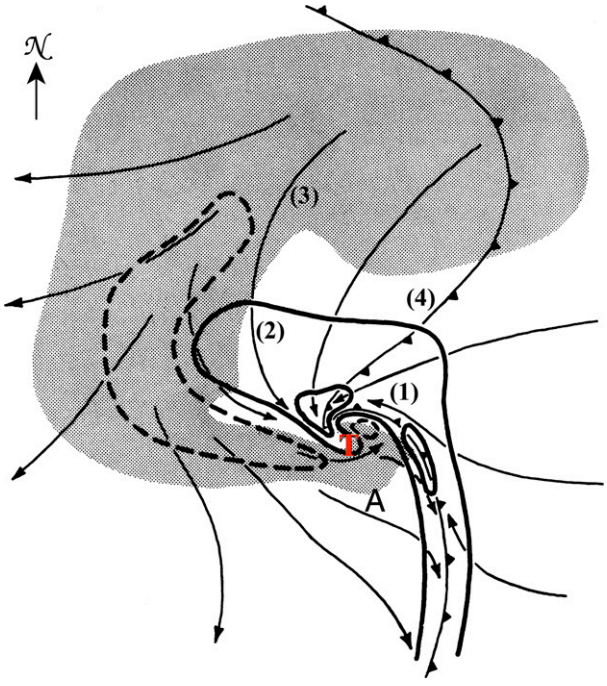

FIG. 2. Schematic flow field near the ground in a tornadic supercell. The stippled region depicts the radar echo. The contours at 2 m s^{-1} intervals are of the vertical-velocity field. The zero contour is omitted and positive (negative) contours are solid (dashed). The flow arrows depict the storm-relative streamlines. The red "T" inside the hook and the black "A" mark the location of a cyclonic tornado and a rare anticyclonic tornado, respectively. Numbers in the figure are as follows: (1) marks the inflow where upward tilting of environmental vorticity is occurring. Along the streamline passing through (3) and (2), the river-bend effect is producing streamwise vorticity from transverse vorticity in left-turning flow; (3) locates the downdraft region where baroclinic generation of horizontal vorticity is occurring near the LFCB; (4) marks a place where horizontal streamwise vorticity is generated baroclinically along the FFDB, which is the front that extends from the vortex northward. The SVC may lie along either the FFDB or the LFCB (adapted from Klemp and Rotunno 1983).

beneath the updraft, tilted toward the vertical, and vertically stretched. As well as generating horizontal vorticity, surface drag also acts to enhance low-level convergence in the mesocyclone by increasing cyclostrophic imbalance and radial inflow.

Based on advanced visualization of their numerical output, Orf et al. (2017) associated tornadoes with preceding and nearby streamwise vorticity currents (SVC), which form along a baroclinic forward-flank downdraft boundary (FFDB) or a left-front convergence boundary (LFCB) (Beck and Weiss 2013; Orf 2019) as depicted in Fig. 2. The tail cloud rising into the wall cloud in Fig. 3 forms along an FFDB or an LFCB. Although the tornado is pendant from the wall cloud and eventually becomes the center of circulation, it forms near an updraft–downdraft interface (Lemon and Doswell 1979). It does not form near the place where the SVC-associated tail cloud ascends into the wall cloud (Fig. 3; Fujita 1959) because

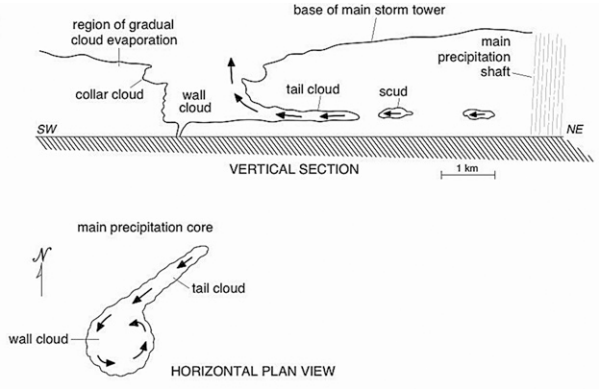

FIG. 3. Vertical section and horizontal plan view of the SVC and associated tail cloud along a boundary (either the FFDB or LFCB). Parcels in the tail cloud acquire baroclinic streamwise vorticity owing to their presence in a transverse buoyancy gradient. This vorticity is tipped upward as the parcels rise into the wall cloud and updraft rotation is enhanced locally. The tornado is located in a gradient of vertical velocity, not in the part of the wall cloud where the SVC and tail cloud enter it (from Fujita 1959).

the vertical vorticity is forming in air as it is rising away from the ground (Davies-Jones 1982). Nevertheless the intersection of the SVC with the updraft is an important location because it is a place at low altitude where the mesocyclonic rotation is enhanced locally owing to upward tilting and stretching of streamwise vorticity, pressure is falling rapidly, the upward pressure-gradient force is powerful, and the updraft is intense due to "vortex suction" (Lilly 1986).

The visualizations accentuate the SVC, but do not show how a tornado obtains its vorticity. Since vorticity is a property of parcels, we must adopt a Lagrangian approach and analyze the vorticity evolution of parcels that enter a tornado. Air only enters a tornado through its corner region close to the ground; it does not enter aloft through its sides. Rotating rain curtains may be instrumental in bringing rotation to the ground. Based on visual evidence, Fujita (1975) proposed the recycling hypothesis for tornado formation. A rotating rain curtain descends around the mesocyclone and initiates a twisting downdraft through drag forces, evaporative cooling, and advection. The torque due to a horizontal hydrometeor gradient of 3.5 g kg^{-1} km^{-1} is roughly the same as that due to a horizontal temperature gradient of 1 K km^{-1}. As this downdraft hits the ground, some of its air flows inwards toward the axis of rotation, thus transporting angular momentum downward and inwards. The near-ground tornado cyclone that results from this spinup intensifies into a tornado as a result of frictional interaction with the ground. An idealized axisymmetric simulation by Davies-Jones (2008, hereafter DJ08) models this process using large raindrops released at the top of the updraft. Animation clearly shows that the tornado forms ground upward and connects with the one aloft as horizontal vorticity is tilted into the vertical and then advected upward in an axial jet. In this regard, the axisymmetric simulation agrees with Orf's high-resolution 3D simulations. The process also produces anticyclonic vorticity adjacent to the tornado as often observed. The vortex aloft does not build gradually downward to the surface by the dynamic pipe effect (Smith and Leslie 1979; Trapp and Davies-Jones 1997).

We should recognize that there is more to tornadogenesis than just identifying the origins of the tornado's vertical vorticity. Updraft rotation aloft plays an important role. Even though rotation near the ground develops baroclinically, frictionally, or as a result of differential hydrometeor drag, it is set up indirectly by the broader updraft rotation aloft, which originates from tilting of streamwise vorticity (DJ84) and leads to rotating rain curtains and left-turning subsiding flow at low elevations. For example, in the DJ08 simulation, azimuthal torque-generated vorticity, although not tilted, is nonetheless important because its associated circulation radically alters the flow in the radial–height plane, resulting in downward and inward transport of angular momentum. Tornadogenesis would not occur in the simulation without it.

To help identify vorticity generation and amplification processes in supercell simulations, previous theoretical work concerning steady isentropic inviscid supercell-like flows (DJ17) is extended herein to unsteady nonisentropic flow. Given the wind field from a supercell simulation, the new work can be used to calculate the partial vorticities of parcels that enter simulated tornadoes and thus to formulate the above ideas about tornadic rotation. The vorticity equation for general flow is integrated in the nonorthogonal Lagrangian coordinates that were used previously by Dahl et al. (2014) to compute a parcel's barotropic vorticity. Dahl et al.'s method is generalized herein to obtain formulas for baroclinic and frictional vorticity as well. For steady flow the new method yields simpler formulas and derivations than the equivalent ones generated by DJ17, using Scorer's (1997, 74–78) secondary-vorticity approach.

Formulas for the barotropic, baroclinic, and frictional vorticities are obtained herein for several kinds of flow. In sections 2 and 3 the flow is very general with Coriolis and friction forces included. In sections 4 and 5, we specify that the reference frame is nonrotating and approximately (or exactly in section 5) storm relative, that the environment is horizontally uniform, and that the supercell-like flow is frictionless. We also turn the Lagrangian horizontal axes with height so that they are streamwise and crosswise to the frame-relative environmental wind. In section 5 the flow is further restricted to being steady, dry, and isentropic. Section 6 demonstrates how easy it is to deduce the relationship between updraft helicity and storm-relative environmental helicity with the techniques developed herein. In appendix B we show that in the limit of steady dry isentropic flow the formulas obtained in section 5 reduce to those obtained laboriously in DJ17. Section 7 uses the formulas to show how rotation may develop in a supercell, and section 8 encapsulates the vorticity-evolution theory.

2. Mathematical formulation

In Earth's rotating reference frame, the equations governing motion, mass continuity, and entropy are

$$\frac{d\mathbf{v}}{dt} + 2\boldsymbol{\Omega} \times \mathbf{v} = T\nabla S - gq_L\nabla z - \nabla(c_pT + \Phi) + \mathbf{F}, \quad (1)$$

$$\frac{d\ln\alpha}{dt} = \nabla \cdot \mathbf{v}, \quad (2)$$

$$\frac{dS}{dt} = \dot{Q}/T \equiv \dot{S}, \quad (3)$$

where t is time, d/dt is the material derivative, $\mathbf{v}$ is the wind vector, $\boldsymbol{\Omega}$ is Earth's angular velocity, Φ is the apparent gravitational potential, $-gq_L\nabla z$ is the drag force (weight) of hydrometeors, g is the acceleration due to gravity, q_L is the hydrometeor mixing ratio, z is height, $\mathbf{F}$ is the friction force per unit mass, T is temperature, S is the specific dry entropy, α is the specific volume (reciprocal of density ρ), c_p and c_v are the specific heats of dry air at constant pressure and constant volume, R is the gas constant for dry air, c_pT is the specific enthalpy, and $\dot{Q}$ is heat per unit mass added to a parcel. In terms of α and T,

$$S = c_v \ln T + R\ln\alpha + \text{const.} \quad (4)$$

Let $\boldsymbol{\omega} \equiv \nabla \times \mathbf{v} + 2\boldsymbol{\Omega}$ denote the absolute vorticity. By taking the curl of (1) and using vector identities and (2), we obtain the following equation in the true vector $\mathbf{w} \equiv \alpha\boldsymbol{\omega}$:

$$L(\mathbf{w}) \equiv \frac{d\mathbf{w}}{dt} - (\mathbf{w} \cdot \nabla)\mathbf{v} = \alpha\nabla \times \mathbf{N} \quad (5)$$

(Dutton 1976, p. 382), where $\mathbf{N} \equiv T\nabla S - gq_L\nabla z + \mathbf{F}$ is the net nonconservative force and $\nabla \times \mathbf{N}$ is the net torque. The barotropic part, $\mathbf{w}_{\rm BT}$, of $\mathbf{w}$ satisfies the homogeneous version (or torque-free version) of (5), namely,

$$L(\mathbf{w}_{\rm BT}) = \frac{d\mathbf{w}_{\rm BT}}{dt} - (\mathbf{w}_{\rm BT} \cdot \nabla)\mathbf{v} = 0, \quad (6)$$

subject to the condition that initially the barotropic vorticity is equal to the total vorticity. Any vector field $\mathbf{B}$ for which $L(\mathbf{B}) = 0$ is frozen into the fluid (Borisenko and Tarapov 1979, p. 240). Thus $\mathbf{w}_{\rm BT}$ is a frozen-in field. Given $\mathbf{v}$ from a numerical simulation and the initial vorticity field, (6) determines $\mathbf{w}_{\rm BT}$.

For later use, we now summarize basic properties of nonorthogonal Lagrangian coordinates. We define right-handed Cartesian coordinates $(x, y, z) \equiv (x^1, x^2, x^3)$ with unit basis vectors $\mathbf{i}$, $\mathbf{j}$, and $\mathbf{k}$, where $\mathbf{i}$ is eastward, $\mathbf{j}$ is northward, and $\mathbf{k}$ $(=\nabla z)$ is vertically upward, respectively. The position vector $\mathbf{x} \equiv x\mathbf{i} + y\mathbf{j} + z\mathbf{k}$ and the wind $\mathbf{v} \equiv u\mathbf{i} + v\mathbf{j} + w\mathbf{k}$. In the Lagrangian framework, $(X, Y, Z, \tau) \equiv (X^1, X^2, X^3, \tau)$ are the independent variables where τ is the Lagrangian time coordinate and the Lagrangian spatial coordinates X, Y, and Z are defined as the Cartesian coordinates at an initial time τ_0 of a parcel that is at the position vector $\mathbf{x}$ at the current time τ. The material derivative $d/dt \equiv \partial/\partial t + \mathbf{v} \cdot \nabla$ in Eulerian coordinates becomes $\partial/\partial\tau$ in Lagrangian coordinates. A parcel trajectory is

$$\mathbf{x}(\tau) = \mathbf{X} + \int_{\tau_0}^{\tau} \mathbf{v}(\mathbf{X}, \sigma)d\sigma, \quad (7)$$

where $\mathbf{X} \equiv (X, Y, Z)$ is the initial position vector of a parcel, σ is a dummy time variable, and $\mathbf{v}(\mathbf{X}, \sigma)$ is the parcel velocity at time σ. The integrals in this paper are Lagrangian ones (following a parcel), for which the integrands should be expressed in Lagrangian coordinates. A numerical simulation provides the wind field $\mathbf{v}$. Following Salmon (1998, p. 5), we define a label space with Cartesian coordinates (X, Y, Z) and a location space with Cartesian coordinates (x, y, z). Parcels are stationary in label space, and move along their trajectories in location space. Alternatively, we can think of the label variables (X, Y, Z) as time-dependent curvilinear coordinates that the flow drags through location space according to the mapping (7).

The material Lagrangian curvilinear system used here is a nonorthogonal coordinate system (Margenau and Murphy 1956, 192–196; D'haeseleer et al. 1991, 7–39) with covariant basis vectors

$$\mathbf{e}_1(\tau) = \frac{\partial\mathbf{x}(\tau)}{\partial X}, \quad \mathbf{e}_2(\tau) = \frac{\partial\mathbf{x}(\tau)}{\partial Y}, \quad \mathbf{e}_3(\tau) = \frac{\partial\mathbf{x}(\tau)}{\partial Z}, \quad (8)$$

where $\mathbf{e}_1(\tau_0) = \mathbf{i}$, $\mathbf{e}_2(\tau_0) = \mathbf{j}$, and $\mathbf{e}_3(\tau_0) = \mathbf{k}$. Hereafter, subscript 0 denotes initial values. By the chain rule, the components of $\mathbf{e}_j(\tau)$ at two different times τ and σ are related by

$$\frac{\partial x^i(\tau)}{\partial X^j} = \frac{\partial x^i(\tau)}{\partial x^k(\sigma)}\frac{\partial x^k(\sigma)}{\partial X^j} \quad (9)$$

in tensor notation with the Einstein summation convention. Thus a covariant basis vector evolves according to

$$\mathbf{e}_j(\tau) = \mathbf{J}(\tau, \sigma)\mathbf{e}_j(\sigma) \quad \text{where } \mathbf{J}(\tau, \sigma) \equiv \partial x^i(\tau)/\partial x^k(\sigma). \quad (10)$$

Here $\mathbf{J}$ is operating as a state-transition matrix (Miller and Michel 1982, 96–97).

In terms of the Lagrangian basis vectors, the equation for continuity or mass conservation is

$$\mathbf{e}_1 \cdot \mathbf{e}_2 \times \mathbf{e}_3 = \frac{\alpha}{\alpha_0}, \quad (11)$$

where $\alpha_0 \equiv \alpha(\tau_0)$ is the initial specific volume and α/α_0 is the dilatation.

The $\mathbf{e}_i(\tau)$ are tangent to the coordinate curves X^i. Note that $\mathbf{e}_1(\tau)$, $\mathbf{e}_2(\tau)$, and $\mathbf{e}_3(\tau)$ are the current configurations of short material line elements attached to a parcel that are initially parallel to the x, y, and z axes. At a point these vectors define a tiny fluid stencil (Fig. 4; Dahl et al. 2014) that evolves in location space as illustrated in Fig. 5. The arms of the stencil are proportional to the covariant basis vectors. Initially they are of uniform length $dX = dY = dZ \equiv \Delta$, and define a tiny cube as shown. The arms are material "elastic strings" that stretch and turn, and the material grid volume deforms into a parallelepiped (Fig. 5) of the same mass as the initial cube (Fig. 4). In label space the cube is naturally static. Equation (11) is a statement that the mass of the material parallelepiped in Fig. 5 is invariant (Lamb 1945, p. 14).

By differentiating (7) with respect to X^i, we find that the covariant basis vectors evolve according to

$$\mathbf{e}_i(\tau) = \mathbf{e}_i(\tau_0) + \int_{\tau_0}^{\tau} \frac{\partial\mathbf{v}(\mathbf{X}, \sigma)}{\partial X^i}\,d\sigma, \quad (12)$$

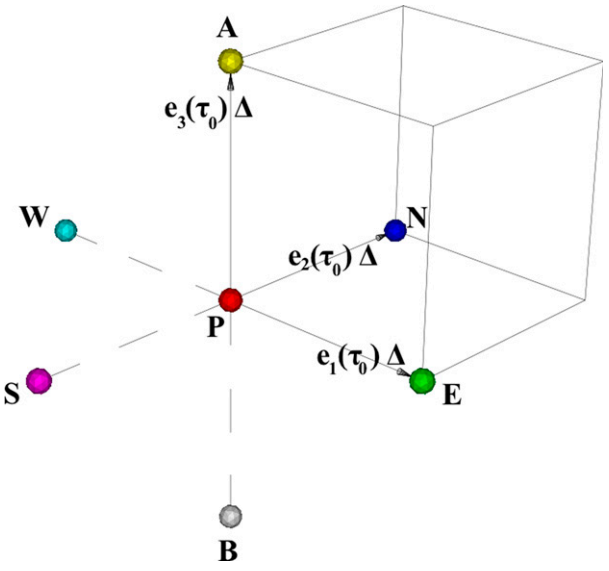

FIG. 4. Perspective view of the parcel stencil and volume at the initial time τ_0. At this time the spacing of the parcels is uniform and equal to Δ. The red ball marks the parcel, and the green, cyan, blue, purple, yellow, and gray balls locate its eastward, westward, northward, southward, upward, and downward neighbors, labeled E, W, N, S, A, and B, respectively. The vectors from the red ball to the green, blue, and yellow balls are the initial covariant basis vectors $\mathbf{e}_1(\tau_0)$, $\mathbf{e}_2(\tau_0)$, and $\mathbf{e}_3(\tau_0)$, which form an orthonormal set times Δ. The triple product $\mathbf{e}_1(\tau_0) \times \mathbf{e}_2(\tau_0) \cdot \mathbf{e}_3(\tau_0)$ is proportional to the volume Δ^3 of the tiny cube. In label space, the stencil and cube are static.

which describes stretching and reorientation of the material line elements.

The contravariant basis vectors $\mathbf{e}^j$ for the Lagrangian coordinates are

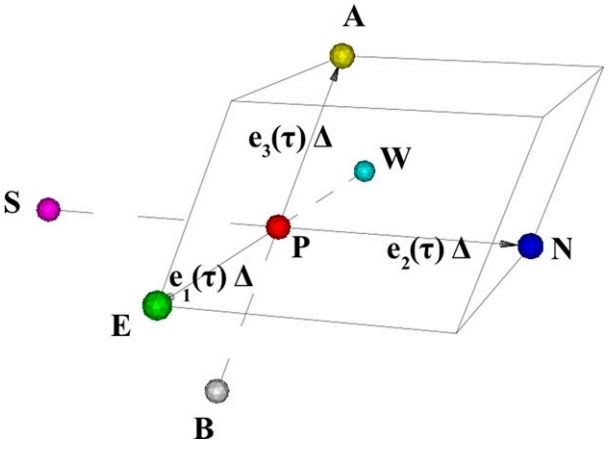

FIG. 5. As in Fig. 4, but at a later time τ. In location space the material stencil is irregular and the tiny cube has deformed into a parallelepiped with the same mass as the original cube. The covariant basis vectors $\mathbf{e}_1(\tau)$, $\mathbf{e}_2(\tau)$, and $\mathbf{e}_3(\tau)$ are no longer unit vectors and are no longer orthogonal to one another.

$$\mathbf{e}^1 = \frac{\alpha_0}{\alpha}\,\mathbf{e}_2 \times \mathbf{e}_3, \quad \mathbf{e}^2 = \frac{\alpha_0}{\alpha}\,\mathbf{e}_3 \times \mathbf{e}_1, \quad \mathbf{e}^3 = \frac{\alpha_0}{\alpha}\,\mathbf{e}_1 \times \mathbf{e}_2 \tag{13}$$

(Margenau and Murphy 1956, p. 193). These are reciprocal to the $\mathbf{e}_i$ ones because, from (13) and (11),

$$\mathbf{e}_i \cdot \mathbf{e}^j = \delta_i^j, \tag{14}$$

where δ_i^j is the Kronecker delta (D'haeseleer et al. 1991, p. 8). Now

$$\begin{aligned}\mathbf{e}_i \cdot \nabla X^j &= \left(\frac{\partial x^1}{\partial X^i}\,\mathbf{i} + \frac{\partial x^2}{\partial X^i}\,\mathbf{j} + \frac{\partial x^3}{\partial X^i}\,\mathbf{k}\right) \cdot \left(\frac{\partial X^j}{\partial x^1}\,\mathbf{i} + \frac{\partial X^j}{\partial x^2}\,\mathbf{j} + \frac{\partial X^j}{\partial x^3}\,\mathbf{k}\right) \\ &= \frac{\partial x^1}{\partial X^i}\,\frac{\partial X^j}{\partial x^1} + \frac{\partial x^2}{\partial X^i}\,\frac{\partial X^j}{\partial x^2} + \frac{\partial x^3}{\partial X^i}\,\frac{\partial X^j}{\partial x^3} = \delta_i^j = \mathbf{e}_i \cdot \mathbf{e}^j\end{aligned} \tag{15}$$

by the chain rule and (14). Hence the contravariant basis vectors are

$$\mathbf{e}^1(\tau) = \nabla X, \quad \mathbf{e}^2(\tau) = \nabla Y, \quad \mathbf{e}^3(\tau) = \nabla Z. \tag{16}$$

The contravariant basis vectors are not material vectors. Instead they are normal to the coordinate surfaces X^i = constant, which are material surfaces. In particular, $\mathbf{e}^3$ is normal to its Z surface, which is the material surface containing all parcels with the same initial height Z, and its magnitude $|\nabla Z|$ measures the local closeness of Z surfaces.

The reciprocals of (11) and (13) are

$$\mathbf{e}^1 \cdot \mathbf{e}^2 \times \mathbf{e}^3 = \frac{\alpha_0}{\alpha}, \tag{17}$$

$$\mathbf{e}_i = \frac{\alpha}{\alpha_0}\,\mathbf{e}^j \times \mathbf{e}^k, \quad (i,j,k)\ \text{circular} \tag{18}$$

(Margenau and Murphy 1956, p. 193), where (i, j, k) circular means that (i, j, k) are circular shifts of (1, 2, 3), namely, (1, 2, 3), (2, 3, 1), (3, 1, 2), for i = 1, 2, 3, respectively. Via (16), (18) becomes

$$\frac{\alpha_0}{\alpha}\,\mathbf{e}_i = \nabla X^j \times \nabla X^k, \quad (i,j,k)\ \text{circular}. \tag{19}$$

By the chain rule and (16), the gradient operator is

$$\nabla \equiv \mathbf{e}^1\,\frac{\partial}{\partial X} + \mathbf{e}^2\,\frac{\partial}{\partial Y} + \mathbf{e}^3\,\frac{\partial}{\partial Z} \equiv \mathbf{e}^i(\tau)\,\frac{\partial}{\partial X^i}. \tag{20}$$

With reciprocal bases, we can represent any vector $\mathbf{A}$ by

$$\mathbf{A} = A_i \mathbf{e}^i = A^i \mathbf{e}_i \tag{21}$$

(D'haeseleer et al. 1991, p. 8), where $A^i \equiv \mathbf{A} \cdot \mathbf{e}^i$ and $A_i \equiv \mathbf{A} \cdot \mathbf{e}_i$ are the contravariant and covariant components of $\mathbf{A}$, respectively. From (14), (20), and (21), we find that

$$\mathbf{A} \cdot \nabla \equiv A^j\,\frac{\partial}{\partial X^j}. \tag{22}$$

From (21), (16), vector identities, and (20), the curl of $\mathbf{A}$ is

$$\nabla \times \mathbf{A} = \nabla \times (A_k \mathbf{e}^k) = \nabla \times (A_k \nabla X^k)$$
$$= \nabla A_k \times \nabla X^k = \nabla A_k \times \mathbf{e}^k = \frac{\partial A_k}{\partial X^j}\, \mathbf{e}^j \times \mathbf{e}^k. \tag{23}$$

Thus in Lagrangian coordinates,

$$\nabla \times \mathbf{A} = \frac{\alpha_0}{\alpha} \sum_{i=1}^{3} \left(\frac{\partial A_k}{\partial X^j} - \frac{\partial A_j}{\partial X^k} \right) \mathbf{e}_i, \quad (i,j,k) \text{ circular}, \tag{24}$$

by (18). Apart from insertion of the continuity Eq. (17), this is the same formula as in D'haeseleer et al. (1991, p. 37). By substituting $\mathbf{A} = a\nabla b$ where a and b are any two differentiable scalars and using (20) and a vector identity, we obtain the useful formula,

$$\alpha \nabla a \times \nabla b = \alpha_0 \left[\frac{\partial(a,b)}{\partial(Y,Z)}\, \mathbf{e}_1 + \frac{\partial(a,b)}{\partial(Z,X)}\, \mathbf{e}_2 + \frac{\partial(a,b)}{\partial(X,Y)}\, \mathbf{e}_3 \right], \tag{25}$$

where

$$\frac{\partial(a,b)}{\partial(X^j,X^k)} \equiv \frac{\partial a}{\partial X^j}\, \frac{\partial b}{\partial X^k} - \frac{\partial a}{\partial X^k}\, \frac{\partial b}{\partial X^j}. \tag{26}$$

3. Integral of the Lagrangian vorticity equation for general flow

Because vorticity is fundamentally a parcel property, we can find a general integral of the vorticity Eq. (5) only in terms of Lagrangian coordinates. Thus we begin our quest for a general integral by obtaining the Lagrangian version of (5). By temporal differentiation of (8) or (12), we see that the $\mathbf{e}_i$ satisfy the differential equation

$$\frac{\partial \mathbf{e}_i}{\partial \tau} = \frac{\partial \mathbf{v}}{\partial X^i}. \tag{27}$$

In Lagrangian coordinates, the quantity $L(\mathbf{w})$ defined in (5) is

$$L(\mathbf{w}) \equiv \frac{d\mathbf{w}}{dt} - (\mathbf{w} \cdot \nabla)\mathbf{v}$$
$$= \frac{\partial(w^1\mathbf{e}_1 + w^2\mathbf{e}_2 + w^3\mathbf{e}_3)}{\partial \tau} - \left(w^1 \frac{\partial}{\partial X^1} + w^2 \frac{\partial}{\partial X^2} + w^3 \frac{\partial}{\partial X^3} \right)\mathbf{v}$$
$$= \frac{\partial w^1}{\partial \tau}\, \mathbf{e}_1 + \frac{\partial w^2}{\partial \tau}\, \mathbf{e}_2 + \frac{\partial w^3}{\partial \tau}\, \mathbf{e}_3, \tag{28}$$

where we have employed (21), (22), and (27). With use of (28) and (24), the differential Eq. (5) for $\mathbf{w} = w^i \mathbf{e}_i$ becomes

$$\frac{\partial w^1}{\partial \tau}\, \mathbf{e}_1(\tau) + \frac{\partial w^2}{\partial \tau}\, \mathbf{e}_2(\tau) + \frac{\partial w^3}{\partial \tau}\, \mathbf{e}_3(\tau) = \alpha_0 \left(\frac{\partial N_3}{\partial Y} - \frac{\partial N_2}{\partial Z} \right) \mathbf{e}_1(\tau)$$
$$+ \alpha_0 \left(\frac{\partial N_1}{\partial Z} - \frac{\partial N_3}{\partial X} \right) \mathbf{e}_2(\tau)$$
$$+ \alpha_0 \left(\frac{\partial N_2}{\partial X} - \frac{\partial N_1}{\partial Y} \right) \mathbf{e}_3(\tau). \tag{29}$$

Henceforth, let subscripts BT, N, BC, q, and F denote barotropic, nonbarotropic, baroclinic, hydrometeor, and frictional, respectively, where N includes all the torques. The total $\mathbf{w} \equiv \alpha\boldsymbol{\omega}$ is the sum of partial vorticities, i.e., $\mathbf{w} = \mathbf{w}_{\rm BT} + \mathbf{w}_{\rm BC} + \mathbf{w}_q + \mathbf{w}_F$ where $\mathbf{w}_{\rm BC} + \mathbf{w}_q + \mathbf{w}_F \equiv \mathbf{w}_N$. From the dot product of the homogeneous version of (29) with $\mathbf{e}^i$ and (14), the initial-value problem (IVP) for the contravariant components of barotropic $\mathbf{w}$ is

$$\frac{\partial w^i_{\rm BT}}{\partial \tau} = 0, \quad w^i_{\rm BT}(\tau_0) = w^i(\tau_0). \tag{30}$$

Similarly from the full version of (29), the IVP for the contravariant components of Lagrangian nonbarotropic vorticity is

$$\frac{\partial w^i_N}{\partial \tau} = \alpha_0 \left(\frac{\partial N_k}{\partial X^j} - \frac{\partial N_j}{\partial X^k} \right), \quad (i,j,k) \text{ circular}, \quad w^i_N(\tau_0) = 0. \tag{31}$$

Note that in contravariant-component form, the Lagrangian vorticity equation is a system of linear inhomogeneous first-order ordinary differential equations with time as the independent variable. Its solution is the sum of the barotropic (homogeneous) solution that satisfies the initial condition on $\mathbf{w}$ and the nonbarotropic (particular) solution that is zero initially.

a. *Barotropic-vorticity formula*

The solution of the IVP (30) is simply

$$w^i_{\rm BT}(\tau) = w^i(\tau_0), \quad i = 1,2,3, \tag{32}$$

and therefore, the formula for vector barotropic $\mathbf{w}$ is

$$\mathbf{w}_{\rm BT}(\tau) \equiv \alpha(\tau)\boldsymbol{\omega}_{\rm BT}(\tau)$$
$$= \alpha_0 \left[\omega^1(\tau_0)\mathbf{e}_1(\tau) + \omega^2(\tau_0)\mathbf{e}_2(\tau) + \omega^3(\tau_0)\mathbf{e}_3(\tau) \right]. \tag{33}$$

This result with the $\mathbf{e}_i$ defined by (8) is Cauchy's formula (Dutton 1976, p. 385; Davies-Jones 2000, 2006, 2015a). The contravariant components of $\mathbf{w}_{\rm BT}$ are just the initial eastward, northward and upward $\mathbf{w}$ components and are thus invariant (Dahl et al. 2014). As expected for a frozen-in field, the initial $\mathbf{w}$ and the current basis vectors determine the current $\mathbf{w}_{\rm BT}$, which is independent of the configurations of the basis vectors at intermediate times. By means of (19), we may write (33) in terms of potentials as

$$\boldsymbol{\omega}_{\rm BT}(\tau) = \omega^1(\tau_0)\nabla Y \times \nabla Z + \omega^2(\tau_0)\nabla Z \times \nabla X + \omega^3(\tau_0)\nabla X \times \nabla Y. \tag{34}$$

From (30) we see that any vector with constant contravariant components satisfies the barotropic-vorticity Eq. (6). Thus the $\mathbf{e}_i(\tau)$, $i = 1, 2, 3$, satisfy (6) individually and the $\mathbf{e}_i$ vectors are therefore material vectors frozen into the fluid [as evident physically from (12)].

b. Formula for nonbarotropic vorticity

By integration, the particular solution of the inhomogeneous IVP (31) is

$$\mathbf{w}_N(\tau) = \alpha_0\mathbf{e}_1(\tau)\int_{\tau_0}^{\tau}\left[\frac{\partial N_3(\sigma)}{\partial Y} - \frac{\partial N_2(\sigma)}{\partial Z}\right]d\sigma + \alpha_0\mathbf{e}_2(\tau)\int_{\tau_0}^{\tau}\left[\frac{\partial N_1(\sigma)}{\partial Z} - \frac{\partial N_3(\sigma)}{\partial X}\right]d\sigma + \alpha_0\mathbf{e}_3(\tau)\int_{\tau_0}^{\tau}\left[\frac{\partial N_2(\sigma)}{\partial X} - \frac{\partial N_1(\sigma)}{\partial Y}\right]d\sigma. \quad (35)$$

By moving the covariant basis vectors in (35) inside the integrals and using (10) and (24), we obtain

$$\mathbf{w}_N(\tau) = \int_{\tau_0}^{\tau}\mathbf{J}(\tau,\sigma)(\alpha\nabla\times\mathbf{N})(\sigma)d\sigma. \quad (36)$$

This formula states that the $\mathbf{w}$ generated by torques in each short time interval $(\sigma, \sigma + d\sigma)$ is brought forward barotropically to the current time τ (i.e., it is frozen in the fluid after generation). The covariant basis vectors account for the effects of subsequent stretching and reorientation on each of these vorticity increments. The total current $\mathbf{w}_N$ is the sum of the stretched contributions from all the small time intervals that span (τ, τ_0) (Davies-Jones 2006).

We observe from (35) that the nonbarotropic vorticity of a parcel depends on the time integral of torques, but not on the specific temporal distribution of the torques within the time interval (τ_0, τ). Thus the timing of the nonbarotropic generation of vorticity relative to tornado formation is immaterial. It can occur mainly near the time of spinup or quite long ago and relatively far from the mesocyclone (Davies-Jones 2015b).

By taking the dot product of (35) with $\mathbf{e}^3$ and using (14) and (24), we see that the nonbarotropic vorticity will have a component normal to the constant-Z surfaces if and only if there is a torque in this direction. Torques associated with turbulence, nonisentropic processes, and/or precipitation can produce vertical vorticity on flat ground (the $Z = 0$ surface).

c. Formulas for the vorticities due to specific torques

The vorticity arising from torques consists of frictional vorticity, baroclinic vorticity, and "hydrometeor vorticity" (vorticity caused by differential hydrometeor drag). The frictional part of $\mathbf{w}$, $\mathbf{w}_F$, is obtained simply by replacing $\mathbf{N}$ in (35) with $\mathbf{F}$. We obtain the baroclinic part $\mathbf{w}_{BC}$ by setting $\mathbf{F} \equiv 0$ and $q_L = 0$. Substituting $T\nabla S$ for $\mathbf{N}$ in (36) and utilizing (25) and (10) yields

$$\mathbf{w}_{BC}(\tau) = \alpha_0\mathbf{e}_1(\tau)\int_{\tau_0}^{\tau}\frac{\partial[T(\sigma),S(\sigma)]}{\partial(Y,Z)}d\sigma + \alpha_0\mathbf{e}_2(\tau)\int_{\tau_0}^{\tau}\frac{\partial[T(\sigma),S(\sigma)]}{\partial(Z,X)}d\sigma + \alpha_0\mathbf{e}_3(\tau)\int_{\tau_0}^{\tau}\frac{\partial[T(\sigma),S(\sigma)]}{\partial(X,Y)}d\sigma. \quad (37)$$

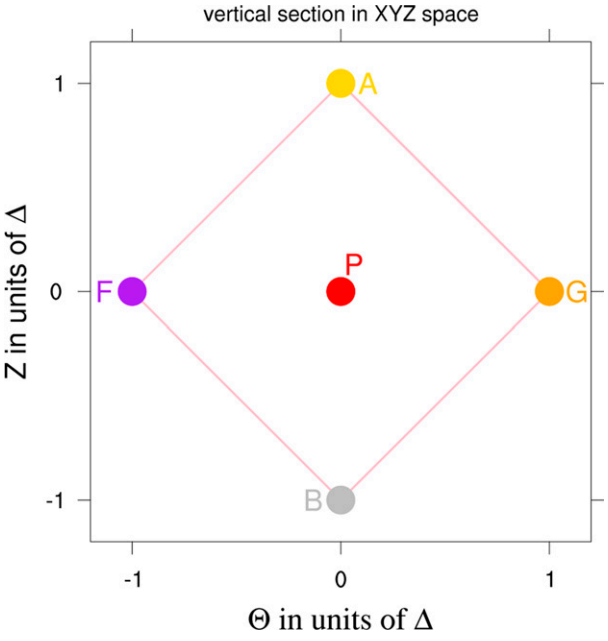

FIG. 6. A vertical section of the stencil in label space. Θ stands for X or Y. The parcels in this section are the central parcel P, its upward (A) and downward (B) neighbors, and two parcels F and G in the stencil that are horizontally aligned with P. In other words FPG can be WPE, EPW, NPS, or SPN, where W, E, N, and S are parcels in Fig. 4. The algebraic area GAFBG is $(\Theta_G Z_A - \Theta_A Z_G + \Theta_A Z_F - \Theta_F Z_A + \Theta_F Z_B - \Theta_B Z_F + \Theta_B Z_G - \Theta_G Z_B)/2$. Its magnitude is $2\Delta^2$.

Using (37) we can compute the baroclinic vorticity of a parcel from its *current* basis vectors and integrals over time of the stencil's T, S material solenoids. We can map the temperature and entropy of stencil parcels onto the T–S plane (or tephigram) and compute each Jacobian as a ratio of areas using algebraic formulas for areas (Davies-Jones 2001). For each solenoid,

$$\frac{\partial(T,S)}{\partial(\Pi,\Xi)} = \frac{\text{enclosed area on tephigram}}{\text{cross-sectional area in initial stencil}} \quad (38)$$

(see Figs. 6 and 7), where (Π, Ξ) stands for (Y, Z), (Z, X), or (X, Y) and the cross-sectional area in the initial stencil (Fig. 6) is simply $2\Delta^2$.

Introducing (19) modifies (37) to

$$\boldsymbol{\omega}_{BC}(\tau) = \nabla Y\times\nabla Z\int_{\tau_0}^{\tau}\frac{\partial[T(\sigma),S(\sigma)]}{\partial(Y,Z)}d\sigma + \nabla Z\times\nabla X\int_{\tau_0}^{\tau}\frac{\partial[T(\sigma),S(\sigma)]}{\partial(Z,X)}d\sigma + \nabla X\times\nabla Y\int_{\tau_0}^{\tau}\frac{\partial[T(\sigma),S(\sigma)]}{\partial(X,Y)}d\sigma. \quad (39)$$

When the flow is isentropic, $S(\tau) = S(\tau_0)$ and the Lagrangian gradients of S can be taken outside the integrals. Then (39) simplifies to

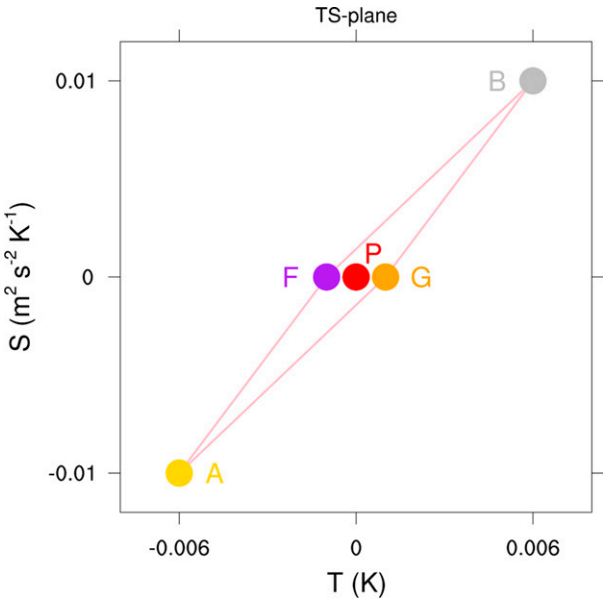

FIG. 7. Temperatures T and entropies S of the neighboring parcels in Fig. 6 plotted on a tephigram. Temperatures and entropies are relative to those of the parcel P. The algebraic area is computed as in Fig. 6, but with T and S replacing Θ and Z, respectively. The case shown is for isentropic flow (for which G and F have the same entropy as P). The signed area in this case, $0.5(T_G - T_F)(S_A - S_B)$, divided by the area in Fig. 6 is equal to the Jacobian $\partial(T, S)/\partial(Y, Z)$.

$$\boldsymbol{\omega}_{BC}(\tau) = \nabla Y \times \nabla Z \frac{\partial[\Lambda(\tau), S(\tau_0)]}{\partial(Y, Z)} + \nabla Z \times \nabla X \frac{\partial[\Lambda(\tau), S(\tau_0)]}{\partial(Z, X)} + \nabla X \times \nabla Y \frac{\partial[\Lambda(\tau), S(\tau_0)]}{\partial(X, Y)}, \tag{40}$$

where

$$\Lambda(\tau) \equiv \int_{\tau_0}^{\tau} T(\sigma) d\sigma \tag{41}$$

is the cumulative temperature. Via the chain rule, (40) simplifies to the formula found by Dutton (1976, p. 390) and Mobbs (1981), namely,

$$\boldsymbol{\omega}_{BC}(\tau) = \nabla\Lambda(\tau) \times \nabla S(\tau_0). \tag{42}$$

In isentropic flow the baroclinic vorticity of a parcel depends on the local gradients of cumulative temperature and entropy.

Replacing T with $-gq_L$ and S with z in (37) results in the formula for "hydrometeor vorticity,"

$$\alpha\boldsymbol{\omega}_q(\tau) = \alpha_0 \mathbf{e}_1(\tau) \int_{\tau_0}^{\tau} \frac{\partial[z(\sigma), gq_L(\sigma)]}{\partial(Y, Z)} d\sigma + \alpha_0 \mathbf{e}_2(\tau) \int_{\tau_0}^{\tau} \frac{\partial[z(\sigma), gq_L(\sigma)]}{\partial(Z, X)} d\sigma + \alpha_0 \mathbf{e}_3(\tau) \int_{\tau_0}^{\tau} \frac{\partial[z(\sigma), gq_L(\sigma)]}{\partial(X, Y)} d\sigma. \tag{43}$$

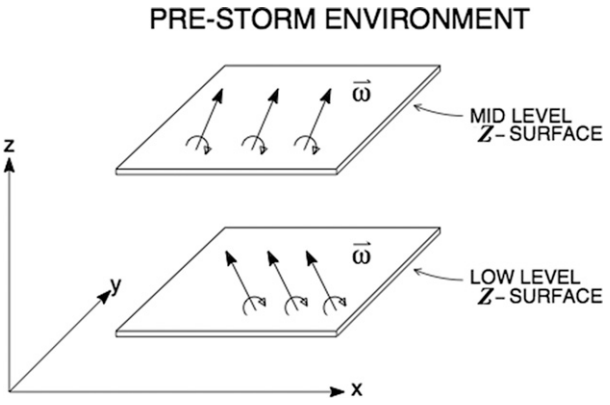

FIG. 8. Schematic of vorticity vectors in surfaces of constant Z in the prestorm or far-upstream environment (adapted from DJ84).

Replacing $-gq_L$ in (43) with b produces a formula for the vorticity associated with a buoyancy force $b\mathbf{k}$.

d. *Constraints that need to be satisfied*

Formulas and diagnostic numerical schemes for parcel trajectories and vorticities should conform to the following rules:

1) To conserve mass, schemes for computing parcel trajectories should satisfy the Lagrangian continuity equation.
2) Schemes for computing parcel trajectories and vorticities should be time reversible. In many Lagrangian trajectory analyses, a parcel's backward trajectory fails to retrace its forward one.
3) All the partial vorticities should be solenoidal.
4) The formulas and schemes should conserve the potential vorticity of a parcel in isentropic motion.
5) They should satisfy circulation theorems.

We verify in appendix A that the formulas developed herein meet requirements 3–5. The formulas satisfy requirement 1 through the continuity equation, Eq. (11), and requirement 2 because (10) is time-reversal invariant owing to the properties of a state-transition matrix (Miller and Michel 1982, p. 96).

4. Unsteady frictionless flow in a horizontally uniform environment

For simplicity, most supercell simulations and theories assume a steady, horizontally uniform, sheared environment over flat ground. Such an environment with veering winds is impossible with Coriolis and/or friction forces (Davies-Jones 2021), so we henceforth set $\boldsymbol{\Omega} = \mathbf{F} = \mathbf{0}$. In a horizontally uniform environment there is no vertical vorticity and the environmental vortex lines are initially horizontal (Fig. 8). Being material lines, the barotropic vortex lines remain in a material surface of constant Z where Z is initial parcel height. Thus the barotropic quantity $\mathbf{w}_{BT} \cdot \nabla Z$ is zero for all time. Since we are assuming no stress at the ground, we can use a reference frame, which moves with a uniform velocity that approximates the storm motion. Henceforth it is understood tacitly

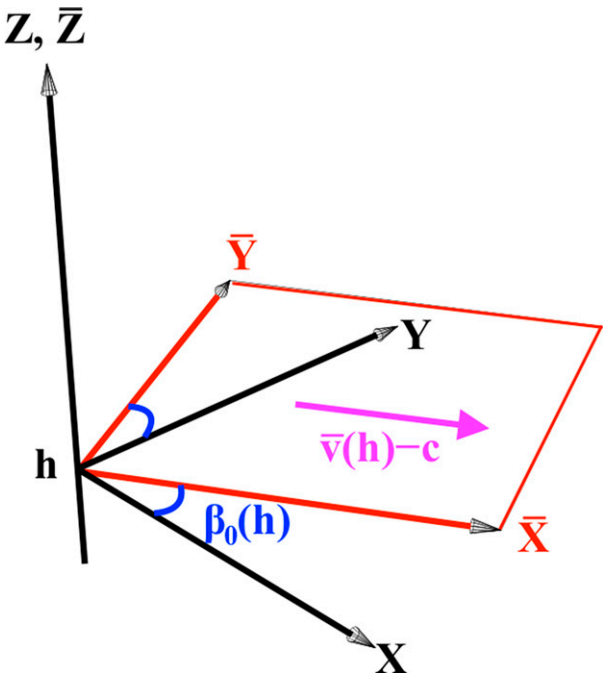

FIG. 9. The coordinate axes at a height h above ground. The Cartesian X, Y, and Z axes are drawn with black arrows. The vertical (Z) axis is not changed. The red arrows depict the new horizontal axes, denoted by overbars, and the red rectangle depicts a part of the horizontal plane at height h. The X axis is twisted through the angle $\beta_0(h)$ shown in blue so that, at each height h, the new X axis (the $\overline{X}$ axis) is parallel to the storm-relative environmental wind [magenta arrow labeled $\overline{\mathbf{v}}(h) - \mathbf{c}$, where $\mathbf{c}$ is the storm-motion vector]. The $\overline{Y}$ axis is horizontal and 90° to the left of the $\overline{X}$ axis.

that all quantities are *frame relative*, not ground relative. We use subscript 0 to denote environmental quantities (apart from use of Z instead of z_0). Thus $T_0(Z)$, $\alpha_0(Z)$, $\boldsymbol{\omega}_0(Z)$, $\mathbf{v}_0(Z)$, $q_0(Z)$, and $\beta_0(Z)$ are the environmental temperature, specific volume, vorticity, wind, wind speed, and direction (to which the wind is blowing, measured counterclockwise from eastward), respectively, and $\mathbf{w}_0(Z) \equiv \alpha_0\boldsymbol{\omega}_0$. These quantities are functions of just Z and are constants of motion because we choose the origin of time τ_0 such that all the parcels in the region of interest at time τ originally start out in the undisturbed horizontally uniform environment.

To aid interpretation, we define new Lagrangian coordinates, denoted by overbars,

$$\begin{aligned} \overline{X} &= X\cos\beta_0(Z) + Y\sin\beta_0(Z), \\ \overline{Y} &= -X\sin\beta_0(Z) + Y\cos\beta_0(Z), \\ \overline{Z} &= Z \end{aligned} \tag{44}$$

so that, in the upstream environment, the lines $\overline{Y}$ = const. and $\overline{X}$ = const. are streamwise and crosswise, respectively, to the frame-relative environmental wind (Fig. 9). This transformation is practical only within Z surfaces because points in different Z surfaces with the same $\overline{X}$ and $\overline{Y}$ are generally widely separated in location space. For use in 3D, we adopt an anholonomic system (Dutton 1976, p. 230) defined in terms of differentials by

$$\begin{aligned} d\overline{X} &= \cos\beta_0\, dX + \sin\beta_0\, dY, \\ d\overline{Y} &= -\sin\beta_0\, dX + \cos\beta_0\, dY, \\ d\overline{Z} &= dZ. \end{aligned} \tag{45}$$

Since the new system depends on knowing Z, and having frictionless flow with a steady storm motion, its use in diagnostic studies of supercell simulations is unworkable. However, it is a useful tool for conceptualizing flows in supercells.

For later use, we now develop important relationships in the new "twisted" system. The inverse transformation is

$$\begin{aligned} dX &= \cos\beta_0\, d\overline{X} - \sin\beta_0\, d\overline{Y}, \\ dY &= \sin\beta_0\, d\overline{X} + \cos\beta_0\, d\overline{Y}, \\ dZ &= d\overline{Z}. \end{aligned} \tag{46}$$

In the twisted system, the covariant basis vectors are

$$\begin{aligned} \overline{\mathbf{e}}_1 &\equiv \frac{\partial\mathbf{x}}{\partial\overline{X}} = \frac{\partial\mathbf{x}}{\partial X}\frac{\partial X}{\partial\overline{X}} + \frac{\partial\mathbf{x}}{\partial Y}\frac{\partial Y}{\partial\overline{X}} = \cos\beta_0\mathbf{e}_1 + \sin\beta_0\mathbf{e}_2, \\ \overline{\mathbf{e}}_2 &\equiv \frac{\partial\mathbf{x}}{\partial\overline{Y}} = \frac{\partial\mathbf{x}}{\partial X}\frac{\partial X}{\partial\overline{Y}} + \frac{\partial\mathbf{x}}{\partial Y}\frac{\partial Y}{\partial\overline{Y}} = -\sin\beta_0\mathbf{e}_1 + \cos\beta_0\mathbf{e}_2, \\ \overline{\mathbf{e}}_3 &\equiv \frac{\partial\mathbf{x}}{\partial\overline{Z}} = \frac{\partial\mathbf{x}}{\partial Z} = \mathbf{e}_3, \end{aligned} \tag{47}$$

by the chain rule, (46), and (8). Initially $\overline{\mathbf{e}}_1$ and $\overline{\mathbf{e}}_2$ are unit vectors that are streamwise and crosswise to the environmental wind $\mathbf{v}_0$. By definition

$$\mathbf{v}_0(Z) = q_0(Z)\overline{\mathbf{e}}_1(\tau_0). \tag{48}$$

We may visualize the vectors $\overline{\mathbf{e}}_1$, $\overline{\mathbf{e}}_2$, and $\overline{\mathbf{e}}_3$ as very short material line elements marked by dye that are initially streamwise, crosswise and vertical to the environmental wind. The flow reorients and stretches or shrinks these material line elements. Since $\mathbf{e}_1 \times \mathbf{e}_2 = \overline{\mathbf{e}}_1 \times \overline{\mathbf{e}}_2$ by (47), the mass continuity equation, (11), becomes

$$\overline{\mathbf{e}}_1 \cdot \overline{\mathbf{e}}_2 \times \overline{\mathbf{e}}_3 = \frac{\alpha}{\alpha_0} \tag{49}$$

in terms of the twisted basis vectors. Inverting (47) provides

$$\begin{aligned} \mathbf{e}_1 &= \cos\beta_0\overline{\mathbf{e}}_1 - \sin\beta_0\overline{\mathbf{e}}_2, \\ \mathbf{e}_2 &= \sin\beta_0\overline{\mathbf{e}}_1 + \cos\beta_0\overline{\mathbf{e}}_2. \end{aligned} \tag{50}$$

The contravariant components of a vector transform according to

$$\overline{A}^i = \frac{\partial\overline{X}^i}{\partial X^j}A^j \tag{51}$$

(Margenau and Murphy 1956, p. 162). Thus from (45)

$$\begin{aligned} \overline{A}^1 &= \cos\beta_0 A^1 + \sin\beta_0 A^2, \\ \overline{A}^2 &= -\sin\beta_0 A^1 + \cos\beta_0 A^2, \\ \overline{A}^3 &= A^3. \end{aligned} \tag{52}$$

From (47) and (52) we obtain the identity

$$\overline{A}^1\bar{\mathbf{e}}_1 + \overline{A}^2\bar{\mathbf{e}}_2 = A^1\mathbf{e}_1 + A^2\mathbf{e}_2. \tag{53}$$

The covariant components of the gradient of a scalar a transform as

$$\frac{\partial a}{\partial X^i} = \frac{\partial a}{\partial \overline{X}^j}\frac{\partial \overline{X}^j}{\partial X^i} \tag{54}$$

by the chain rule (Margenau and Murphy 1956, p. 162). Hence from (45)

$$\begin{aligned}
\frac{\partial a}{\partial X} &= \cos\beta_0\,\frac{\partial a}{\partial \overline{X}} - \sin\,\beta_0\,\frac{\partial a}{\partial \overline{Y}},\\
\frac{\partial a}{\partial Y} &= \sin\beta_0\,\frac{\partial a}{\partial \overline{X}} + \cos\,\beta_0\,\frac{\partial a}{\partial \overline{Y}},\\
\frac{\partial a}{\partial Z} &= \frac{\partial a}{\partial \overline{Z}}.
\end{aligned} \tag{55}$$

Via the identity (55) for general scalars a and b,

$$\begin{aligned}
\frac{\partial(a,b)}{\partial(Y,Z)} &= \cos\beta_0\frac{\partial(a,b)}{\partial(\overline{Y},\overline{Z})} - \sin\,\beta_0\frac{\partial(a,b)}{\partial(\overline{Z},\overline{X})},\\
\frac{\partial(a,b)}{\partial(Z,X)} &= \sin\beta_0\frac{\partial(a,b)}{\partial(\overline{Y},\overline{Z})} + \cos\,\beta_0\frac{\partial(a,b)}{\partial(\overline{Z},\overline{X})},\\
\frac{\partial(a,b)}{\partial(X,Y)} &= \frac{\partial(a,b)}{\partial(\overline{X},\overline{Y})}.
\end{aligned} \tag{56}$$

From (56) and (50) we find that

$$\begin{aligned}
\frac{\partial(a,b)}{\partial(Y,Z)}\mathbf{e}_1 + \frac{\partial(a,b)}{\partial(Z,X)}\mathbf{e}_2 + \frac{\partial(a,b)}{\partial(X,Y)}\mathbf{e}_3 &= \frac{\partial(a,b)}{\partial(\overline{Y},\overline{Z})}\bar{\mathbf{e}}_1 + \frac{\partial(a,b)}{\partial(\overline{Z},\overline{X})}\bar{\mathbf{e}}_2\\
&\quad + \frac{\partial(a,b)}{\partial(\overline{X},\overline{Y})}\bar{\mathbf{e}}_3.
\end{aligned} \tag{57}$$

Thus we obtain from (25),

$$\alpha\nabla a\times\nabla b = \alpha_0\left[\frac{\partial(a,b)}{\partial(\overline{Y},\overline{Z})}\bar{\mathbf{e}}_1 + \frac{\partial(a,b)}{\partial(\overline{Z},\overline{X})}\bar{\mathbf{e}}_2 + \frac{\partial(a,b)}{\partial(\overline{X},\overline{Y})}\bar{\mathbf{e}}_3\right] \tag{58}$$

in the twisted system. From (45) $\partial\overline{Y}/\partial Z = 0$. Hence $\nabla\overline{Y} = \nabla_Z\overline{Y}$ and similarly for $\overline{X}$. Therefore, special cases of (58) are

$$\begin{aligned}
\alpha\nabla_Z\overline{Y}\times\nabla\overline{Z} &= \alpha_0\bar{\mathbf{e}}_1,\\
\alpha\nabla\overline{Z}\times\nabla_Z\overline{X} &= \alpha_0\bar{\mathbf{e}}_2.
\end{aligned} \tag{59}$$

where ∇_Z is the gradient operator with Z held constant.

Furthermore, by the chain rule,

$$\bar{\mathbf{e}}_i\cdot\nabla\overline{X}^j = \frac{\partial x^k}{\partial\overline{X}^i}\frac{\partial\overline{X}^j}{\partial x^k} = \frac{\partial\overline{X}^j}{\partial\overline{X}^i} = \delta_i^j. \tag{60}$$

Thus

$$\begin{aligned}
\bar{\mathbf{e}}_1\cdot\nabla a &= \bar{\mathbf{e}}_1\cdot\left(\frac{\partial a}{\partial\overline{X}}\nabla\overline{X} + \frac{\partial a}{\partial\overline{Y}}\nabla\overline{Y} + \frac{\partial a}{\partial\overline{Z}}\nabla\overline{Z}\right) = \frac{\partial a}{\partial\overline{X}},\\
\bar{\mathbf{e}}_2\cdot\nabla a &= \bar{\mathbf{e}}_2\cdot\left(\frac{\partial a}{\partial\overline{X}}\nabla\overline{X} + \frac{\partial a}{\partial\overline{Y}}\nabla\overline{Y} + \frac{\partial a}{\partial\overline{Z}}\nabla\overline{Z}\right) = \frac{\partial a}{\partial\overline{Y}}.
\end{aligned} \tag{61}$$

Henceforth overbars will be suppressed where they are superfluous as, for example, in $\overline{Z}$, $\overline{A}^3$, and $\bar{\mathbf{e}}_3$. We use (58) in sections 4b and 4d, (59) in sections 4a and 4c, and (61) in appendix B.

a. *Barotropic-vorticity formula*

Substituting the identity (53) into the barotropic-vorticity formula (33) yields

$$\mathbf{w}_{\mathrm{BT}}(\tau) = \alpha_0\left[\overline{\omega}^1(\tau_0)\bar{\mathbf{e}}_1(\tau) + \overline{\omega}^2(\tau_0)\bar{\mathbf{e}}_2(\tau) + \omega^3(\tau_0)\mathbf{e}_3(\tau)\right]. \tag{62}$$

The initial (environmental) components of $\mathbf{w}$ in the streamwise, crosswise and vertical directions are

$$\overline{w}^1(\tau_0) = -\alpha_0 q_0\frac{d\beta_0}{dZ},\quad \overline{w}^2(\tau_0) = \alpha_0\frac{dq_0}{dZ},\quad w^3(\tau_0) = 0 \tag{63}$$

(DJ84). Inserting (63) into (62) produces

$$\mathbf{w}_{\mathrm{BT}}(\tau) = -\alpha_0 q_0\frac{d\beta_0}{dZ}\bar{\mathbf{e}}_1(\tau) + \alpha_0\frac{dq_0}{dZ}\bar{\mathbf{e}}_2(\tau). \tag{64}$$

The static contravariant components in (64) are α_0 times the environmental streamwise and crosswise vorticity. By being frozen in the fluid and thereby taking parcel deformation into account, the vectors $\bar{\mathbf{e}}_1$ and $\bar{\mathbf{e}}_2$ in this formula propagate $\mathbf{w}_{\mathrm{BT}}$ through time. For $\tau > \tau_0$, $\bar{\mathbf{e}}_1(\tau)$ and $\bar{\mathbf{e}}_2(\tau)$ are usually oblique to one another, which is vital for the river-bend effect (see section 5). Note that without knowledge of the instantaneous wind direction, we cannot deduce the *local* streamwise and transverse vorticities when the flow is unsteady. To complicate matters there is even a wind component out of the Z surfaces owing to their movement. Use of (59) provides the following alternative version of (64):

$$\boldsymbol{\omega}_{\mathrm{BT}}(\tau) = -q_0\frac{d\beta_0}{dZ}\nabla_Z\overline{Y}(\tau)\times\nabla Z(\tau) + \frac{dq_0}{dZ}\nabla Z(\tau)\times\nabla_Z\overline{X}. \tag{65}$$

As in the steady-flow case (DJ17), the barotropic vorticity $\boldsymbol{\omega}_{\mathrm{BT}}$ consists of two partial vorticities $\boldsymbol{\omega}_{\mathrm{BTIS}}$ and $\boldsymbol{\omega}_{\mathrm{BTIC}}$ that depend on the imported streamwise and crosswise vorticity, respectively. From (64) and (65) they are

$$\boldsymbol{\omega}_{\mathrm{BTIS}}(\tau) = -\frac{\alpha_0}{\alpha}\,q_0\frac{d\beta_0}{dZ}\bar{\mathbf{e}}_1(\tau) = \nabla_Z\chi_{\mathrm{BTIS}}\times\nabla Z, \tag{66}$$

$$\boldsymbol{\omega}_{\mathrm{BTIC}}(\tau) = \frac{\alpha_0}{\alpha}\,\frac{dq_0}{dZ}\bar{\mathbf{e}}_2(\tau) = \nabla_Z\chi_{\mathrm{BTIC}}\times\nabla Z, \tag{67}$$

where

$$\chi_{\mathrm{BTIS}} \equiv -q_0\frac{d\beta_0}{dZ}\,\overline{Y},\quad \chi_{\mathrm{BTIC}} \equiv -\frac{dq_0}{dZ}\,\overline{X}. \tag{68}$$

The equations of the (frozen-in-the-fluid) vortex lines of $\boldsymbol{\omega}_{\mathrm{BTIS}}$ and $\boldsymbol{\omega}_{\mathrm{BTIC}}$ are $\chi_{\mathrm{BTIS}} = \text{const.}$, $Z = \text{const.}$, and $\chi_{\mathrm{BTIC}} = \text{const.}$, $Z = \text{const.}$, respectively. Thus the vortex lines of imported streamwise vorticity in a given Z surface are the material lines $\overline{Y} = \text{const.}$, which for unsteady flow are

generally parallel to the flow just in the environment. Only in steady flow is $\boldsymbol{\omega}_{\mathrm{BTIS}}$ always streamwise within the storm. Note that the barotropic quantities χ_{BTIS} and χ_{BTIC} are "streamfunctions" for the corresponding partial vorticities ω_{BTIS} and ω_{BTIC}, so within a Z surface the vortex-line spacing is proportional to the vorticity magnitude. Furthermore, they are both conserved following a parcel, similar to angular momentum in frictionless axisymmetric flows (e.g., DJ08).

b. Formula for baroclinic vorticity

By following the same steps that led to (28) but in the new coordinates, we find that

$$L(\mathbf{w}) = \frac{\partial \overline{w}^1}{\partial \tau}\,\overline{\mathbf{e}}_1 + \frac{\partial \overline{w}^2}{\partial \tau}\,\overline{\mathbf{e}}_2 + \frac{\partial w^3}{\partial \tau}\,\mathbf{e}_3. \tag{69}$$

The baroclinic $\mathbf{w}$ equation is therefore

$$\frac{\partial \overline{w}^1}{\partial \tau}\,\overline{\mathbf{e}}_1 + \frac{\partial \overline{w}^2}{\partial \tau}\,\overline{\mathbf{e}}_2 + \frac{\partial w^3}{\partial \tau}\,\mathbf{e}_3 = \alpha_0\left[\overline{\mathbf{e}}_1\,\frac{\partial(T,S)}{\partial(\overline{Y},Z)} + \overline{\mathbf{e}}_2\,\frac{\partial(T,S)}{\partial(Z,\overline{X})} + \overline{\mathbf{e}}_3\,\frac{\partial(T,S)}{\partial(\overline{X},\overline{Y})}\right], \tag{70}$$

where the right side is the baroclinic generation vector $\alpha\nabla T \times \nabla S$ by the identity (58). Integrating (70) with zero initial condition provides the baroclinic vorticity

$$\begin{aligned}\mathbf{w}_{\mathrm{BC}}(\tau) = {}& \alpha_0\overline{\mathbf{e}}_1(\tau)\int_{\tau_0}^{\tau}\frac{\partial\left[T(\sigma),S(\sigma)\right]}{\partial(\overline{Y},Z)}\,d\sigma \\ &+ \alpha_0\overline{\mathbf{e}}_2(\tau)\int_{\tau_0}^{\tau}\frac{\partial\left[T(\sigma),S(\sigma)\right]}{\partial(Z,\overline{X})}\,d\sigma \\ &+ \alpha_0\mathbf{e}_3(\tau)\int_{\tau_0}^{\tau}\frac{\partial\left[T(\sigma),S(\sigma)\right]}{\partial(\overline{X},\overline{Y})}\,d\sigma.\end{aligned} \tag{71}$$

c. Formula for baroclinic vorticity in isentropic flow

Assuming isentropic dry flow simplifies the above formula for baroclinic vorticity, while having no effect on barotropic vorticity. The constant-Z surfaces, which exist by themselves in a homentropic (constant-S) atmosphere, coincide with the isentropic surfaces $S(Z)$ = const. for frictionless isentropic flow in a stratified horizontally uniform environment. The entropy gradient becomes simply

$$\nabla S = \frac{dS}{dZ}\,\nabla Z. \tag{72}$$

Since dS/dZ is constant following a parcel, (71) reduces to

$$\mathbf{w}_{\mathrm{BC}}(\tau) = \alpha_0\left[\overline{\mathbf{e}}_1(\tau)\,\frac{\partial\Lambda(\tau)}{\partial\overline{Y}} - \overline{\mathbf{e}}_2(\tau)\,\frac{\partial\Lambda(\tau)}{\partial\overline{X}}\right]\frac{dS}{dZ}, \tag{73}$$

where Λ is defined by (41). Here we can define Λ as

$$\Lambda(\tau) \equiv \int_{\tau_0}^{\tau} T'(\sigma)\,d\sigma, \tag{74}$$

where $T' \equiv T(\tau) - T_0(Z)$ since $T_0(Z)$ does not affect the derivatives of Λ in (73); T' is the excess temperature of a parcel relative to its environmental temperature far upstream where it is generally at a different height. Owing to compression (expansion), the excess temperature is positive (negative) if the parcel's pressure is greater (less) than its original value. Typically higher (lower) pressure equates to lower (greater) height.

The PV, $\mathbf{w}\cdot(dS/dZ)\nabla Z$, is zero for this flow because $\mathbf{w}_{\mathrm{BT}}\cdot\nabla Z = 0$ from (66) and (67), and $\mathbf{w}_{\mathrm{BC}}\cdot\nabla S = 0$ by (72) and (73). Consequently the barotropic and baroclinic vorticity vectors are confined to the Z surfaces and vertical vorticity cannot exist at the ground.

In isentropic flow, there is a "streamfunction" χ_{BC} for baroclinic vorticity, which satisfies $\nabla_Z\chi_{\mathrm{BC}}\times\nabla Z = \boldsymbol{\omega}_{\mathrm{BC}}$. By introducing (59) into (73) and simplifying via the chain rule, we find that $\boldsymbol{\omega}_{\mathrm{BC}} = \nabla_Z(\Lambda dS/dZ)\times\nabla Z$ and hence

$$\chi_{\mathrm{BC}} = \Lambda dS/dZ. \tag{75}$$

The baroclinic torque generates χ_{BC}. In our idealized flow that mimics an isolated supercell, the baroclinic vortex lines form within the storm and thus cannot extend to infinity within finite time. They are contained within isentropic surfaces and cannot end at the ground, which itself is an isentropic surface in isentropic flow. Since baroclinic vorticity is a source-free field, the baroclinic vortex lines must therefore form closed loops (Davies-Jones 2000; DJ17).

d. Total relative vorticity in isentropic flow

In unsteady isentropic frictionless flow in a horizontally uniform environment,

$$\begin{aligned}\chi &\equiv \chi_{\mathrm{BTIS}} + \chi_{\mathrm{BTIC}} + \chi_{\mathrm{BC}} \\ &= -q_0\,\frac{d\beta_0}{dZ}\,\overline{Y} - \frac{dq_0}{dZ}\,\overline{X} + \Lambda\,\frac{dS}{dZ}\end{aligned} \tag{76}$$

from (68) and (75). Hence the total relative vorticity is

$$\begin{aligned}\boldsymbol{\omega} \equiv \nabla_Z\chi\times\nabla Z &= \nabla_Z\left(-q_0\,\frac{d\beta_0}{dZ}\,\overline{Y}\right)\times\nabla Z + \nabla_Z\left(-\frac{dq_0}{dZ}\,\overline{X}\right)\times\nabla Z + \nabla_Z\left(\Lambda\,\frac{dS}{dZ}\right)\times\nabla Z \\ &= -q_0\,\frac{d\beta_0}{dZ}\,\nabla_Z\overline{Y}\times\nabla Z - \frac{dq_0}{dZ}\,\nabla_Z\overline{X}\times\nabla Z + \frac{dS}{dZ}\,\nabla_Z\Lambda\times\nabla Z.\end{aligned} \tag{77}$$

The three terms on the right side are, in order, the three partial vorticities, $\boldsymbol{\omega}_{\mathrm{BTIS}}$, $\boldsymbol{\omega}_{\mathrm{BTIC}}$, and $\boldsymbol{\omega}_{\mathrm{BC}}$.

This equation for unsteady flow is the same as the one derived by DJ17 [his Eq. (83)] for steady flow. (In the DJ17 notation, $\nabla_Z\overline{Y}$ is ∇n_0 and $\nabla_Z\overline{X}$ is $q_0\nabla_Z E$.) Now (58) with $a = \chi$ and $b = \overline{Z}$ yields

$$\boldsymbol{\omega} \equiv \nabla_Z\chi\times\nabla Z = \frac{\alpha_0}{\alpha}\left(\frac{\partial\chi}{\partial\overline{Y}}\,\overline{\mathbf{e}}_1 - \frac{\partial\chi}{\partial\overline{X}}\,\overline{\mathbf{e}}_2\right). \tag{78}$$

Inserting (76) into (78) yields an equivalent version of (77), namely,

$$\mathbf{w}(\tau) = \alpha\boldsymbol{\omega}(\tau) = \alpha_0\left[-q_0\frac{d\beta_0}{dZ} + \frac{\partial\Lambda(\tau)}{\partial\overline{Y}}\frac{dS}{dZ}\right]\overline{\mathbf{e}}_1(\tau) + \alpha_0\left[\frac{dq_0}{dZ} - \frac{\partial\Lambda(\tau)}{\partial\overline{X}}\frac{dS}{dZ}\right]\overline{\mathbf{e}}_2(\tau). \quad (79)$$

If a parcel spends enough time in a temperature gradient, its baroclinic vorticity can exceed its barotropic vorticity. We can estimate this time by order-of-magnitude analyses of the terms in (79). For $q_0 \sim 10$ m s^{-1}, $d\beta_0/dZ \sim 30°$ km^{-1}, and $dq_0/dZ \sim 5$ m s^{-1} km^{-1}, the environmental streamwise and crosswise vorticity are both $\sim 5 \times 10^{-3}$ s^{-1}. For a lifted index of -6 K, $dS/dZ \sim -4 \times 10^{-3}$ m s^{-2} K^{-1}. Assuming that the parcel is in a Lagrangian temperature gradient of 1 K km^{-1}, the Lagrangian gradient of Λ at time τ is 10^{-3} $(\tau - \tau_0)$ K s m^{-1}. Hence its baroclinic vorticity is 4×10^{-6} $(\tau - \tau_0)$ s^{-1}. Thus the parcel's baroclinic vorticity may exceed its barotropic vorticity in as little as 20 min. This conclusion is consistent with the findings of Rotunno and Klemp (1985) and others.

5. Steady frictionless dry isentropic flow in a horizontally uniform environment

As storms in sheared environments evolve into supercells, they become more organized and quasi steady. In special situations (environments with circular hodographs and neutral stratification), steady, inviscid, homentropic, supercell-like solutions (Beltrami flows) exist (Lilly 1982; DJ08). Supercells actually exhibit some Beltrami-like properties (Lilly 1982, 1986). Even though supercells are never completely steady, cyclic supercell simulations (e.g., Adlerman et al. 1999) may be quasi-steady numerical solutions that orbit quasi periodically in phase space around a fixed point. We now postulate that our supercell-like flow has attained a steady state in the frame moving with the storm so that we can discover its properties, which a quasi-steady solution will share approximately. Incidentally we recover nicer but equivalent versions of the formulas in DJ17 as demonstrated in appendix B.

We assume that all parcels flow through the storm from the horizontally uniform environment, none are trapped in a gyre within the storm. The parcels now follow streamlines, which, like the vortex lines, lie in the static Z surfaces. As in DJ17, we define the streamwise, transverse, and binormal directions as the ones aligned locally with the 3D wind, 90° to the left of this wind in the local Z surface, and upward normal to the Z surface, respectively. In the environment, transverse is the same as crosswise. In steady flow, each parcel remains on a single streamline for all time because the trajectories coincide with the streamlines. Hence, physical interpretation is simplified because the material line elements $\overline{\mathbf{e}}_1$ that are streamwise in the environment stay streamwise in the 3D sense. Thus we can find formulas for the local streamwise and transverse vorticities (the binormal vorticity is zero). Note that the material-line elements $\overline{\mathbf{e}}_2$ and $\overline{\mathbf{e}}_3$ do not stay normal to the streamlines and Z surfaces, respectively.

The steady-state assumption is advantageous because it yields a simple expression for the wind. Since $\partial\mathbf{v}/\partial t = 0$ in the storm-relative frame,

$$\frac{\partial\mathbf{v}}{\partial\tau} - (\mathbf{v}\cdot\nabla)\mathbf{v} = 0 \Rightarrow L(\mathbf{v}) = 0, \quad (80)$$

so $\mathbf{v}$ now satisfies $L(\mathbf{B}) = 0$. The result of (80) that satisfies the initial condition, $\mathbf{v}(\tau_0) = q_0(Z)\overline{\mathbf{e}}_1(\tau_0)$ is

$$\mathbf{v}(\tau) = q_0(Z)\overline{\mathbf{e}}_1(\tau), \quad (81)$$

so in steady flow the contravariant wind components are static with two of them vanishing. As well as being the vortex lines of $\boldsymbol{\omega}_{\mathrm{BTIS}}$, the material lines defined by $\overline{Y}$ = const. and Z = const., are now streamlines. If we assume that a storm inflow is barotropic, the storm-relative helicity density of incoming parcels is

$$\mathbf{v}\cdot\boldsymbol{\omega}_{\mathrm{BT}} = \frac{\alpha_0}{\alpha}q_0\left(-q_0\frac{d\beta_0}{dZ}\right)\overline{\mathbf{e}}_1\cdot\overline{\mathbf{e}}_1 + \frac{\alpha_0}{\alpha}q_0\frac{dq_0}{dZ}\overline{\mathbf{e}}_1\cdot\overline{\mathbf{e}}_2 \quad (82)$$

from (81) and (79). Since $\mathbf{v} = q\mathbf{t}$, where q is the parcel's speed and $\mathbf{t}$ is the unit tangent in its direction of motion (both in the updraft's reference frame), (81) implies that

$$\overline{\mathbf{e}}_1 = q\mathbf{t}/q_0. \quad (83)$$

Inserting (83) into (82) yields

$$\mathbf{v}\cdot\boldsymbol{\omega}_{\mathrm{BT}} = \frac{\alpha_0}{\alpha}q^2\left(-\frac{d\beta_0}{dZ}\right) + \frac{\alpha_0}{\alpha}q\frac{dq_0}{dZ}\mathbf{t}\cdot\overline{\mathbf{e}}_2. \quad (84)$$

If, in the environment, the storm-relative directional shear is large compared to the speed shear, the first term on the right dominates the second one, and the storm-relative helicity density of a parcel in confluent inflow should increase as the square of its storm-relative wind speed. This explains Wade et al.'s (2018) observations of storm-relative helicity in the accelerating inflows of supercells increasing with proximity to the updraft.

From (B15) in appendix B we find that the streamwise vorticity of a parcel in steady flow is

$$\boldsymbol{\omega}\cdot\mathbf{t} = \underbrace{R\frac{dZ}{db}\left(-q_0\frac{d\beta_0}{dZ}\right)}_{A} + \underbrace{R\frac{dZ}{db}\left(\frac{\partial\Lambda}{\partial\overline{Y}}\frac{dS}{dZ}\right)}_{B} + \underbrace{\boldsymbol{\omega}\cdot\mathbf{n}\cot\phi}_{C}, \quad (85)$$

where ϕ is the angle between $\overline{\mathbf{e}}_1$ and $\overline{\mathbf{e}}_2$, and R, dZ, and db are defined in appendix B. Of consequence here is the nondimensional combination RdZ/db. Its value is one when the parcel is the environment. It increases as the streamline spacing and closeness of isentropic surfaces decrease in the parcel's vicinity. By the continuity Eq. (B6), RdZ/db equals the parcel's momentum magnitude ρq divided by its momentum magnitude far upstream. Hence, term A represents streamwise stretching acting on environmental streamwise vorticity. Likewise term B describes streamwise stretching of the parcel's

accumulated streamwise baroclinic vorticity. Term C is the river-bend effect described next.

Figure 1 illustrates flow of a river around a left-hand bend (Shapiro 1972; Scorer 1997; Adlerman et al. 1999; Davies-Jones et al. 2001). Upstream of the bend where the flow is straight, the flow speed increases with height owing to drag exerted by the river bottom. Here there is positive transverse vorticity, and no streamwise and binormal vorticity. The binormal vorticity remains zero around the bend so anticyclonic shear vorticity cancels cyclonic curvature vorticity, resulting in faster (slower) flow around the inside (outside) of the bend. From a vorticity perspective, streamwise vorticity develops owing to $\mathbf{v}(r)$ turning the primary transverse vorticity streamwise. In terms of basis vectors, the turning of $\bar{\mathbf{e}}_2$ toward $\bar{\mathbf{e}}_1$ produces streamwise vorticity. In a supercell, streamwise vorticity is produced in this manner in the left-turning flow in the outer part of the mesocyclone where the angular velocity decreases outwards. The force perspective is as follows. Owing to Bernoulli's principle, pressure is low (high) at the inside (outside). As in boundary layers for instance, pressure varies less with height than wind speed. Consequently, the faster (slower) fluid at top (bottom) moves outward (inward) because of excess centrifugal force (pressure-gradient force).

6. Updraft rotation

The vertical component of vorticity is intrinsic to rotating updrafts. Rotunno (1981) found an integral of the *inhomogeneous* vertical-vorticity equation, which depends on integration of the tilting and stretching terms along a parcel trajectory. Barotropic vorticity depends only on the initial and current configurations of the fluid material and is independent of intermediate configurations (Davies-Jones 2006) so there exists a simpler vertical-vorticity formula, which we now obtain. Let $h(X, Y, \tau)$ be the height of a particular Z surface. From $\mathbf{k}\cdot$(64) and $\mathbf{k}\cdot$(47) we find that the barotropic vertical vorticity in a Z surface is given by

$$\frac{\alpha}{\alpha_0}\,\zeta_{\mathrm{BT}}(\tau) = -q_0\,\frac{d\beta_0}{dZ}\,\frac{\partial h(\tau)}{\partial \overline{X}} + \frac{dq_0}{dZ}\,\frac{\partial h(\tau)}{\partial \overline{Y}}. \tag{86}$$

Thus the barotropic vertical vorticity depends on the environmental vorticity and the horizontal gradient with respect to *Lagrangian* coordinates of the height of the Z surface. Clearly (86) is the nonlinear compressible extension of Eq. (20) in DJ84 and is the fully nonlinear version of Eq. (7) in Rotunno and Klemp (1985) and Eq. (5.7) in Kanehisa (2002). The main difference between (86) and previous versions is that the Lagrangian horizontal coordinates replace the Eulerian ones.

For steady flow we can derive a relationship relating updraft rotation to environmental helicity. From $\mathbf{k}\cdot$(81) and $\mathbf{k}\cdot$(47), the vertical velocity w (not to be confused with $\mathbf{w}$ or its components with indices) on a Z surface is simply

$$w = q_0\,\frac{\partial h}{\partial \overline{X}}. \tag{87}$$

Hence for steady flow (86) becomes

$$\alpha\zeta_{\mathrm{BT}} = -\alpha_0\,\frac{d\beta_0}{dZ}\,w + \alpha_0\,\frac{dq_0}{dZ}\,\frac{\partial h}{\partial \overline{Y}}. \tag{88}$$

With environmental winds veering with height and without speed shear, there is perfect correlation between $\alpha\zeta_{\mathrm{BT}}$ and w with $-\alpha_0\ d\beta_0/dZ$ as the constant of proportionality (the abnormality). By multiplying (88) by w, given by (87), we obtain

$$\frac{\alpha}{\alpha_0}\,w\zeta_{\mathrm{BT}} = q_0\left(-q_0\,\frac{d\beta_0}{dZ}\right)\frac{\partial h}{\partial \overline{X}}\,\frac{\partial h}{\partial \overline{X}} + q_0\,\frac{dq_0}{dZ}\,\frac{\partial h}{\partial \overline{X}}\,\frac{\partial h}{\partial \overline{Y}}. \tag{89}$$

As shown above, in steady flow $\overline{Y}$ is proportional to a streamfunction. For any flow with left–right symmetry in the direction of the storm-relative flow, the average value across an updraft of the last term in (89) is clearly zero. Then integrating (89) over an updraft's cross-sectional area A produces

$$\int\!\!\int_A \alpha w\zeta_{\mathrm{BT}}\,dA \approx \alpha_0(\bar{\mathbf{v}} - \mathbf{c})\cdot\boldsymbol{\omega}\int\!\!\int_A\left(\frac{\partial h}{\partial \overline{X}}\right)^2 dA. \tag{90}$$

Here $\bar{\mathbf{v}}$ is the *ground*-relative environmental wind, $\mathbf{c}$ is the storm motion, and $\bar{\mathbf{v}} - \mathbf{c} \equiv \mathbf{v}_0$. Thus we expect quasi-circular updrafts to rotate significantly as a whole when the storm-relative environmental helicity density $(\bar{\mathbf{v}} - \mathbf{c})\cdot\boldsymbol{\omega}$ is large (Davies-Jones et al. 1990; Droegemeier et al. 1993). This is the same conclusion as reached from Eq. (23) in DJ84 except for a finite-amplitude steady updraft instead of for an infinitesimal and exponentially growing disturbance. Kanehisa (2002) obtained a similar result. As demonstrated in DJ84 (see his Fig. 9), the relationship (90) can be invalid for certain quasi-linear updrafts.

7. Application to rotation in supercells

In this section, we apply the formulas to show how rotation about a vertical axis can develop in a supercell. For brevity, "vorticity" in this section does not distinguish between $\boldsymbol{\omega}$ (vorticity) and $\mathbf{w}$ (specific volume times vorticity). The 3D vorticity arising from imported crosswise vorticity is most important in environmental storm-relative winds with large speed shear. It is equal to the environmental crosswise vorticity times the initially crosswise vector $\bar{\mathbf{e}}_2$ [see (67)]. Lifting of imported crosswise vorticity on the right (left) side of an initial updraft gives rise to cyclonic (anticyclonic) rotation there (Fig. 10; Rotunno and Klemp 1982, 1985; Klemp 1987). From (66), the 3D vorticity arising from imported streamwise vorticity is equal to the environmental streamwise vorticity times the initially streamwise vector $\bar{\mathbf{e}}_1$. Significant rotation develops where $\bar{\mathbf{e}}_1$ is stretched and tilted upward. Thus overall updraft rotation of the main storm tower stems from stretching in the storm inflow and lifting by the updraft of imported streamwise vorticity (Fig. 11) in environments with strong low-level storm-relative winds that veer markedly with height.

When applying the formula (71) for baroclinic vorticity, recall that, owing to the dominant effect of compressional warming (expansional cooling), a parcel that is at a lower

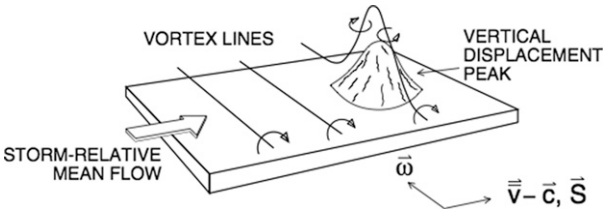

FIG. 10. How rotation occurs in updrafts when the environmental vorticity is crosswise. Lifting of environmental vortex lines over a peak in a Z surface results in cyclonic (anticyclonic) rotation on the right (left) side of the peak with no overall updraft rotation (from DJ84).

(higher) height than its environmental height generally has a higher (lower) temperature than its environmental temperature (DJ17). Moreover, S decreasing with Z is necessary for isentropic flow in our analytical model to have warm updrafts and cool downdrafts. The third term on the right of (71) is the component of vorticity produced normal to a Z surface by integrated solenoids within the material surface. In dry, frictionless, isentropic flow with horizontally uniform environments, this term is absent and there is no way to obtain rotation about a vertical axis at the ground.

The baroclinic mechanism is most important at low elevations for two reasons. First of all, flow along a baroclinic zone into an updraft enhances updraft rotation. Consider a parcel flowing in the SVC along a boundary toward the wall cloud (Figs. 2, 3) with its $\bar{\mathbf{e}}_1$ string streamwise. If the environmental wind in the parcel's isentropic surface is mainly in this direction, the $\overline{Y}$ direction is left of the boundary. Further suppose subsidence to the right of the boundary. Since $dS/dZ < 0$ for static instability and $\left(\partial T/\partial \overline{Y}\right)_Z < 0$ here, the parcel's time integral of the Jacobian $\partial(T,S)/\partial(\overline{Y},Z)$ in (71) is positive and the parcel acquires streamwise vorticity baroclinically as it travels in the baroclinic zone and cyclonic vorticity as it rises into the updraft (Rotunno and Klemp 1985). Where the SVC enters the updraft, there is a local increase in rotation with

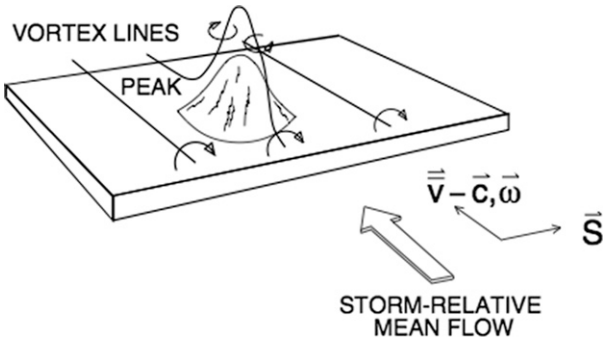

FIG. 11. How updraft rotation occurs when the environmental vorticity is streamwise. As parcels flow across a peak in a constant-Z surface, their streamwise vorticity is tilted. The maximum vertical velocity and vertical vorticity are both located on the upstream side of the peak, resulting in overall cyclonic updraft rotation (from DJ84).

associated decrease in pressure and increase in updraft velocity at low levels (Orf et al. 2017) as discussed in section 1.

The second reason is the direct role baroclinic generation plays in tornadogenesis (DJ17). Consider a parcel descending along an isentropic surface in unstable stratification. In this situation $\left(\partial T/\partial \overline{X}\right)_Z > 0$ owing to compressional warming and $\partial(T,S)/\partial(Z,\overline{X})$ is positive. Hence, the second term on the right in (71) produces positive transverse baroclinic vorticity. For this air to rotate cyclonically as it is lifted, transverse vorticity must be turned streamwise by the river-bend effect. The descending parcel acquires streamwise vorticity by being turned leftward (outside the mesocyclone's core of solid-body rotation) by the mesocyclone's inward pressure-gradient force. By mass continuity, isentrope packing and streamline confluence also occurs in the subsiding quickening current. As the parcel exits the rear-flank downdraft and accelerates along the ground toward the storm updraft, its 3D streamwise vorticity grows due to streamwise stretching [lengthening of $\bar{\mathbf{e}}_1$ in (71)]. Vortex suction (Lilly 1986) then lifts the cool parcel into the updraft. Upward tilting and vertical stretching of its 3D streamwise vorticity greatly increases rotation near the ground. Upward advection of vertical vorticity intensifies rotation and induces lowering pressure aloft (as in an animation of the DJ08 simulation). This produces further increases in low-level convergence and vortex suction. This positive-feedback process results in a strong tornado cyclone. Frictional interaction with the ground causes the tornado cyclone to contract and spin up into a tornado.

8. Summary of vorticity-evolution theory

The most significant formulas, many of which are new, are cited in this section. We can conceptualize the Lagrangian dynamics as a configuration of material strings (the covariant basis vectors) multiplied by mathematical coefficients or weights (the contravariant components). The covariant basis vectors, $\mathbf{e}_1$, $\mathbf{e}_2$, and $\mathbf{e}_3$, attached to each parcel are tiny material vectors that turn and stretch or shrink elastically with the flow. Initially they form an orthonormal set of vectors with $\mathbf{e}_1$ and $\mathbf{e}_2$ horizontal and $\mathbf{e}_3$ upward. A general vector is a weighted sum of its covariant basis vectors. For a material vector, the weights are static and the strings propagate a parcel's material vector through time via the "frozen-field" effect. Thus, a material vector at the current time depends only on its initial value and the current strings. It is independent of the string configurations at intermediate times. The barotropic $\mathbf{w}$ vector, given by either (33) or (34), is a material vector.

The general formulas for baroclinic vorticity are (37) or (39). In contrast to the constant weights of barotropic $\mathbf{w}$, the weights of baroclinic $\mathbf{w}$ are time dependent and zero initially. They are the temporal integrals from the initial to current times of the contravariant components of the baroclinic generation vector $\alpha\nabla T \times \nabla S$. The frictional vorticity, given by (35) with $\mathbf{F}$ instead of $\mathbf{N}$, is similar to the baroclinic vorticity except the generation vector is frictional instead of baroclinic. Owing to large vertical gradients of stress, the generation of

frictional vorticity near the ground is predominantly horizontal. For precipitating convection, there is also a partial vorticity owing to hydrometeor drag [see (43)]. In left-turning flow with positive speed shear in the Northern Hemisphere, the river-bend effect produces 3D streamwise vorticity from all types (barotropic, baroclinic, frictional, and hydrometeor) of transverse vorticity (Fig. 1).

To model frictionless supercell-like flows, we assume a horizontally uniform environment with Z surfaces that are either level initially or, for steady flow, level far upstream and that all quantities are storm relative. It is now convenient to define a new set of covariant basis vectors, $\bar{\mathbf{e}}_1$, $\bar{\mathbf{e}}_2$, and $\mathbf{e}_3$, such that $\bar{\mathbf{e}}_1$ and $\bar{\mathbf{e}}_2$ are initially parallel and left normal to the environmental wind. These too are tiny material vectors that are attached to each parcel. The initially streamwise and transverse strings $\bar{\mathbf{e}}_1$ and $\bar{\mathbf{e}}_2$ are tangent to the material Z surfaces. The static weights of barotropic $\mathbf{w}$, given by (63), are now the environmental streamwise and crosswise $\mathbf{w}$ since a parcel starts out in a horizontally uniform environment. In unsteady flow, we cannot deduce the streamwise vorticity of a parcel easily because there is no simple relationship between its instantaneous flow direction and its basis vectors. Like in the steady-flow case (DJ17), the total relative vorticity $\boldsymbol{\omega}$ in unsteady frictionless dry flow consists of three partial vorticities, two barotropic parts, $\boldsymbol{\omega}_{\mathrm{BTIS}}$ and $\boldsymbol{\omega}_{\mathrm{BTIC}}$, that depend on imported streamwise and crosswise vorticity, respectively, and a baroclinic part, $\boldsymbol{\omega}_{\mathrm{BC}}$. These are given by (66), (67), and (71).

Assuming isentropic flow simplifies the formulas for baroclinic vorticity as illustrated by (73). For frictionless, isentropic, supercell-like flow, the potential vorticity is zero. Since the ground is an isentropic surface, there can be no vertical vorticity at flat ground. To obtain vertical vorticity at ground level when there is none there initially, torques must generate vorticity in the $\mathbf{e}_3$ direction, which is never tangential to the Z surfaces. For this to happen, potential vorticity must be produced by drag forces or diabatic heating or cooling.

In steady flow, the wind $\mathbf{v}$ equals $q_0\bar{\mathbf{e}}_1$ and is a material vector. The parcel trajectories are then streamlines, which are also lines of streamwise vorticity. Thus the imported streamwise vorticity remains streamwise within the storm. The formula for streamwise vorticity in steady, isentropic, frictionless flow is (85). In left-curving steady flow, turning of $\bar{\mathbf{e}}_2$ toward $\bar{\mathbf{e}}_1$ produces 3D streamwise vorticity from transverse vorticity.

An algorithm for computing partial vorticities along time-reversible trajectories will be presented in a future paper. This algorithm is based on the methodology and formulas developed in section 3 and satisfies the five conditions in section 3d. It has been tested on an analytical flow with an exact solution.

Acknowledgments. Dr. Qin Xu's thorough review of the original manuscript is gratefully acknowledged. Comments by the three anonymous reviewers resulted in vastly improved clarification and organization. NOAA/National Severe Storms Laboratory paid the publication fees.

Data availability statement. No datasets were generated or analyzed during the present study.

APPENDIX A

Formula Checks

First we check that each partial vorticity satisfies the basic prerequisite of being solenoidal. From (18) and (16), $\mathbf{e}_i\,\alpha_0/\alpha = \mathbf{e}^j \times \mathbf{e}^k = \boldsymbol{\nabla}X^j \times \boldsymbol{\nabla}X^k = \boldsymbol{\nabla} \times (X^j\boldsymbol{\nabla}X^k)$ is nondivergent. By this fact, vector identities, (20) and (14), the Lagrangian formula for divergence is

$$\boldsymbol{\nabla}\cdot\boldsymbol{\omega} = \boldsymbol{\nabla}\cdot\left(\frac{\alpha}{\alpha_0}\,\omega^i\,\frac{\alpha_0}{\alpha}\mathbf{e}_i\right) = \frac{\alpha_0}{\alpha}\,\mathbf{e}_i\cdot\boldsymbol{\nabla}\left(\frac{\alpha}{\alpha_0}\,\omega^i\right) + \frac{\alpha}{\alpha_0}\,\omega^i\boldsymbol{\nabla}\cdot\cancel{\left(\frac{\alpha_0}{\alpha}\mathbf{e}_i\right)}$$

$$= \frac{\alpha_0}{\alpha}\,\mathbf{e}_i\cdot\mathbf{e}^j\,\frac{\partial}{\partial X^j}\left(\frac{\alpha}{\alpha_0}\,\omega^i\right) = \frac{\alpha_0}{\alpha}\,\frac{\partial}{\partial X^i}\left(\frac{\alpha}{\alpha_0}\,\omega^i\right) \tag{A1}$$

D'haeseleer et al. (1991, p. 36). Thus a partial vorticity $\boldsymbol{\omega}_-$ is solenoidal if

$$0 = \frac{\alpha}{\alpha_0}\,\boldsymbol{\nabla}\cdot\boldsymbol{\omega}_- = \frac{\partial}{\partial X^i}\left(\frac{\mathbf{w}_-\cdot\mathbf{e}^i}{\alpha_0}\right) \tag{A2}$$

since $\mathbf{w}_- \equiv \alpha\boldsymbol{\omega}_-$. For barotropic vorticity

$$\frac{\partial}{\partial X^i}\left[\frac{\mathbf{w}_{\mathrm{BT}}(\tau)\cdot\mathbf{e}^i}{\alpha_0}\right] = \frac{\partial}{\partial X^i}\left[\omega^i(\tau_0)\right] \tag{A3}$$

from (33). Therefore $\boldsymbol{\omega}_{\mathrm{BT}}$ is solenoidal since the initial vorticity is solenoidal. From (35) and (14),

$$\frac{\partial}{\partial X^i}\left[\frac{\mathbf{w}_N(\tau)\cdot\mathbf{e}^i(\tau)}{\alpha_0}\right] = \frac{\partial}{\partial X}\int_{\tau_0}^{\tau}\left[\frac{\partial N_3(\sigma)}{\partial Y} - \frac{\partial N_2(\sigma)}{\partial Z}\right]d\sigma$$
$$+ \frac{\partial}{\partial Y}\int_{\tau_0}^{\tau}\left[\frac{\partial N_1(\sigma)}{\partial Z} - \frac{\partial N_3(\sigma)}{\partial X}\right]d\sigma \tag{A4}$$
$$+ \frac{\partial}{\partial Z}\int_{\tau_0}^{\tau}\left[\frac{\partial N_2(\sigma)}{\partial X} - \frac{\partial N_1(\sigma)}{\partial Y}\right]d\sigma = 0$$

by cancellation of terms so the partial vorticities associated with torques are also solenoidal.

Second we show that the formulas for vorticity are consistent with the circulation theorems. The vector element of surface area in the X^i direction is $d\mathbf{A}_i(\tau) = \mathbf{e}_j(\tau)\times\mathbf{e}_k(\tau)\,dX^j dX^k$, $(i, j, k$ circular) (Margenau and Murphy 1956, p. 194). From the above, (33), and (11), the barotropic circulation around a material curve $C(\tau)$ that encloses an area $A(\tau)$ is

$$\Gamma_{\mathrm{BT}} \equiv \int\int_{A(\tau)}\boldsymbol{\omega}_{\mathrm{BT}}(\tau)\cdot d\mathbf{A}(\tau)$$
$$= \int\int_{A(\tau_0)}\left[\omega^1(\tau_0)dY\,dZ + \omega^2(\tau_0)dZ\,dX + \omega^3(\tau_0)dX\,dY\right]. \tag{A5}$$

Thus the barotropic circulation is conserved (Kelvin's circulation theorem). Similarly from (35) the nonbarotropic circulation is

$$\Gamma_N(\tau) = \int\int_{A(\tau_0)} \int_{\tau_0}^{\tau} \sum_{i=1}^{3} \left[\frac{\partial N_k(\sigma)}{\partial X^j} - \frac{\partial N_j(\sigma)}{\partial X^k} \right] d\sigma\, dX^j\, dX^k \quad (i,j,k) \text{ circular},$$
$$= \int_{\tau_0}^{\tau} \oint_{C(\tau_0)} \left[N_1(\sigma) dX + N_2(\sigma) dY + N_3(\sigma) dZ \right] d\sigma = \int_{\tau_0}^{\tau} \oint_{C(\tau_0)} \mathbf{N}(\sigma) \cdot d\mathbf{X}\, d\sigma \tag{A6}$$

after changing the order of integration and using Stokes theorem. Consistent with Dutton (1976, 372–373), the nonbarotropic circulation is the integral over time of the circulation of the net nonconservative force around the material curve.

Third we demonstrate that in dry isentropic and frictionless flow, potential vorticity (PV) $\mathbf{w} \cdot \nabla S$ is conserved. From (20)

$$\nabla S = \mathbf{e}^j(\tau) \frac{\partial S}{\partial X^j}, \tag{A7}$$

so the covariant components of ∇S are static for any conserved variable S. Therefore, from the dot product of (33) with (A7) and (14), we find that

$$\mathbf{w}_{\mathrm{BT}} \cdot \nabla S = \alpha_0 w^j_{\mathrm{BT}}(\tau_0) \frac{\partial S}{\partial X^j} \tag{A8}$$

is conserved. Because the $\partial S/\partial X^i$ are constants of the motion and can be taken outside the integrals in (37), it is easily proven from the dot product of (37) with (A7) and (14) that

$$\mathbf{w}_{\mathrm{BC}} \cdot \nabla S = 0. \tag{A9}$$

Hence the formulas are compatible with PV conservation.

APPENDIX B

Agreement of Current Formulas with Those in DJ17

To reconcile present formulas for steady flow with those derived in DJ17, we define a right-handed set of orthonormal basis vectors ($\mathbf{t}$, $\mathbf{n}$, $\mathbf{b}$), where $\mathbf{t}$, $\mathbf{n}$, and $\mathbf{b}$ are in the streamwise, transverse, and binormal directions. By definition $\mathbf{v} = q\mathbf{t}$, where q is the storm-relative wind speed. In general, $\bar{\mathbf{e}}_1$ and $\mathbf{t}$ are in different directions. For steady flow, however,

$$\bar{\mathbf{e}}_1 = (q/q_0)\mathbf{t} = \mathbf{v}/q_0 \tag{B1}$$

from (81). Since $\bar{\mathbf{e}}_2(\tau)$ is a material line whose endpoints are always on the same two streamlines and $\bar{\mathbf{e}}_2(\tau_0)$ is a unit vector normal to the environmental streamlines,

$$\bar{\mathbf{e}}_2(\tau) \cdot \mathbf{n} = 1/R(\tau), \tag{B2}$$

where $1/R$ is the ratio of the streamline spacing in a parcel's current locality to the spacing in the parcel's vicinity when it was in the far-upstream environment. By (B2) and simple trigonometry $\bar{\mathbf{e}}_2 \cdot \mathbf{t} = \cot\phi/R$, where ϕ is the angle between $\bar{\mathbf{e}}_2$ and $\mathbf{t}$. Therefore

$$\bar{\mathbf{e}}_2 = (\bar{\mathbf{e}}_2 \cdot \mathbf{t})\mathbf{t} + (\bar{\mathbf{e}}_2 \cdot \mathbf{n})\mathbf{n} = \frac{\cot\phi}{R}\mathbf{t} + \frac{1}{R}\mathbf{n}. \tag{B3}$$

Next we derive the continuity equation used in DJ17 from formulas in this paper. From (B1) and (B3),

$$\bar{\mathbf{e}}_1 \times \bar{\mathbf{e}}_2 = \frac{q}{q_0}\frac{1}{R}\mathbf{b}, \tag{B4}$$

since $\mathbf{b} = \mathbf{t} \times \mathbf{n}$. Hence by the continuity equation, Eq. (49),

$$\frac{q}{q_0}\frac{1}{R}\mathbf{b} \times \mathbf{e}_3 = \frac{\alpha}{\alpha_0}. \tag{B5}$$

Physically this states that the mass of a material parallelepiped such as in Figs. 4 and 5 is invariant. Note that $\mathbf{b} \cdot \bar{\mathbf{e}}_3 \equiv db/dZ$ is the ratio of the spacing of Z surfaces in a parcel's vicinity, denoted by db, to the local spacing when it was in the environment, denoted by dZ. Thus

$$R\frac{dZ}{db} = \frac{q}{q_0}\frac{\alpha_0}{\alpha}, \tag{B6}$$

which is Eq. (42) in DJ17. Equation (B6) equates streamline spacing and closeness of isentropic surfaces in a parcel's surroundings to its streamwise stretching and dilatation or, alternatively, to the ratio of its current momentum magnitude ρq to its value when it was in the environment.

To obtain the formula for the transverse-vorticity component $\boldsymbol{\omega} \cdot \mathbf{n}$ of a parcel in DJ17, we take the dot product of (79) with $\mathbf{n}$ and use (B1) and (B2). This gives

$$\boldsymbol{\omega} \cdot \mathbf{n}(\tau) = \frac{\alpha_0}{\alpha(\tau)}\frac{1}{R(\tau)}\left[\frac{dq_0}{dZ} - \frac{\partial\Lambda(\tau)}{\partial\overline{X}}\frac{dS}{dZ}\right]. \tag{B7}$$

Next we differentiate (74) with respect to time. For steady flow this yields

$$T'(\tau) = \frac{\partial\Lambda}{\partial\tau} = \cancel{\frac{\partial\Lambda}{\partial t}} + \mathbf{v} \cdot \nabla\Lambda = q_0\bar{\mathbf{e}}_1 \cdot \nabla\Lambda = q_0\frac{\partial\Lambda}{\partial\overline{X}} \tag{B8}$$

via (B1) and (61). With (B8), (B7) becomes

$$\boldsymbol{\omega} \cdot \mathbf{n} = \frac{\alpha_0}{\alpha(\tau)}\frac{1}{R(\tau)}\left[\frac{\frac{dq_0}{dZ} - T'(\tau)}{q_0}\frac{dS}{dZ}\right], \tag{B9}$$

which is Eq. (89) in DJ17.

We rediscover the DJ17 formula for streamwise vorticity as follows. Taking the dot product of (79) with $\mathbf{t}$ yields the following formula for the streamwise-vorticity vector $(\boldsymbol{\omega} \cdot \mathbf{t})\mathbf{t}$ in steady frictionless dry isentropic flow in a horizontally uniform environment:

$$\frac{\alpha(\tau)}{\alpha_0}(\boldsymbol{\omega}\cdot\mathbf{t})\mathbf{t}=\left[-q_0\frac{d\beta_0}{dZ}+\frac{\partial\Lambda(\tau)}{\partial\overline{Y}}\frac{dS}{dZ}\right][\bar{\mathbf{e}}_1(\tau)\cdot\mathbf{t}]\mathbf{t}+\left[\frac{dq_0}{dZ}-\frac{\partial\Lambda(\tau)}{\partial\overline{X}}\frac{dS}{dZ}\right][\bar{\mathbf{e}}_2(\tau)\cdot\mathbf{t}]\mathbf{t}. \quad \text{(B10)}$$

After substituting for $\bar{\mathbf{e}}_1$ from (B1), (B10) becomes

$$\frac{\alpha}{\alpha_0}(\boldsymbol{\omega}\cdot\mathbf{t})\mathbf{t}=\left[-\frac{d\beta_0}{dZ}+\frac{1}{q_0}\frac{\partial\Lambda}{\partial\overline{Y}}\frac{dS}{dZ}+\frac{\bar{\mathbf{e}}_2\cdot\mathbf{t}}{q}\left(\frac{dq_0}{dZ}-\frac{\partial\Lambda}{\partial\overline{X}}\frac{dS}{dZ}\right)\right]\mathbf{v}. \quad \text{(B11)}$$

In DJ17 notation,

$$\frac{\delta_\perp\Lambda}{\delta_\perp n_0}\equiv\frac{\mathbf{n}}{R}\cdot\nabla\Lambda=\left[\bar{\mathbf{e}}_2-\frac{q_0}{q}(\bar{\mathbf{e}}_2\cdot\mathbf{t})\bar{\mathbf{e}}_1\right]\cdot\nabla\Lambda=\frac{\partial\Lambda}{\partial\overline{Y}}-\frac{q_0}{q}(\bar{\mathbf{e}}_2\cdot\mathbf{t})\frac{\partial\Lambda}{\partial\overline{X}} \quad \text{(B12)}$$

by (B3), (B1), and (61). Note that (B12) is true for any differentiable scalar, not just Λ. DJ17 introduced a variable E, which we need to relate to quantities used in this paper. The lines $E=$ const. are isochrones because E is the elapsed time since a parcel passed a "starting line" $\overline{X}=$ const. in the far upstream environment. By this definition, $E=\overline{X}/q_0+$ const. so $\partial E/\partial\overline{Y}=0$ and $\partial E/\partial\overline{X}=1/q_0$. Thus (B12) with E instead of Λ gives us

$$\frac{\delta_\perp E}{\delta_\perp n_0}\equiv\frac{\mathbf{n}}{R}\cdot\nabla E=-\frac{\bar{\mathbf{e}}_2\cdot\mathbf{t}}{q}. \quad \text{(B13)}$$

Note that λ_0 in DJ17 is $-d\beta_0/dZ$ in this paper. Inserting (B12), (B13), and λ_0 in (B11) yields

$$\frac{\alpha}{\alpha_0}(\boldsymbol{\omega}\cdot\mathbf{t})\mathbf{t}=\left(\lambda_0-\frac{\delta_\perp E}{\delta_\perp n_0}\frac{dq_0}{dZ}+\frac{1}{q_0}\frac{\delta_\perp\Lambda}{\delta_\perp n_0}\frac{dS}{dZ}\right)\mathbf{v}, \quad \text{(B14)}$$

which is Eq. (90) in DJ17.

Last, we find a version of the streamwise-vorticity equation that is useful for physical interpretation (see section 5). By introducing (B1), (B7), (B3), and (B6) into (B10), we obtain

$$\boldsymbol{\omega}\cdot\mathbf{t}=\frac{\alpha_0}{\alpha}\frac{q}{q_0}\left(-q_0\frac{d\beta_0}{dZ}+\frac{\partial\Lambda}{\partial\overline{Y}}\frac{dS}{dZ}\right)+\boldsymbol{\omega}\cdot\mathbf{n}\cot\phi=R\frac{dZ}{db}\left(-q_0\frac{d\beta_0}{dZ}+\frac{\partial\Lambda}{\partial\overline{Y}}\frac{dS}{dZ}\right)+\boldsymbol{\omega}\cdot\mathbf{n}\cot\phi. \quad \text{(B15)}$$

REFERENCES

Adlerman, E. J., K. K. Droegemeier, and R. Davies-Jones, 1999: A numerical simulation of cyclic mesocyclogenesis. *J. Atmos. Sci.*, **56**, 2045–2069, https://doi.org/10.1175/1520-0469(1999)056<2045:ANSOCM>2.0.CO;2.

Batchelor, G. K., 1967: *An Introduction to Fluid Dynamics*. Cambridge University Press, 615 pp.

Beck, J., and C. Weiss, 2013: An assessment of low-level baroclinity and vorticity within a simulated supercell. *Mon. Wea. Rev.*, **141**, 649–669, https://doi.org/10.1175/MWR-D-11-00115.1.

Borisenko, A. I., and I. E. Tarapov, 1979: *Vector and Tensor Analysis with Applications*. Dover, 257 pp.

Dahl, J. M. L., 2015: Near-ground rotation in simulated supercells: On the robustness of the baroclinic mechanism. *Mon. Wea. Rev.*, **143**, 4929–4942, https://doi.org/10.1175/MWR-D-15-0115.1.

——, M. D. Parker, and L. J. Wicker, 2014: Imported and storm-generated near-ground vertical vorticity in a simulated supercell. *J. Atmos. Sci.*, **71**, 3027–3051, https://doi.org/10.1175/JAS-D-13-0123.1.

Davies-Jones, R. P., 1982: Observational and theoretical aspects of tornadogenesis. *Intense Atmospheric Vortices*, L. Bengtsson and J. Lighthill, Eds., Springer-Verlag, 175–189.

——, 1984: Streamwise vorticity: The origin of updraft rotation in supercell storms. *J. Atmos. Sci.*, **41**, 2991–3006, https://doi.org/10.1175/1520-0469(1984)041<2991:SVTOOU>2.0.CO;2.

——, 2000: A Lagrangian model for baroclinic genesis of mesoscale vortices. Part I: Theory. *J. Atmos. Sci.*, **57**, 715–736, https://doi.org/10.1175/1520-0469(2000)057<0715:ALMFBG>2.0.CO;2.

——, 2001: Computation of a solenoid as a ratio of areas and a geometric interpretation of the Arakawa Jacobian. *Mon. Wea. Rev.*, **129**, 345–353, https://doi.org/10.1175/1520-0493(2001)129<0345:COASAA>2.0.CO;2.

——, 2006: Integrals of the vorticity equation. Part I: General three- and two-dimensional flows. *J. Atmos. Sci.*, **63**, 598–610, https://doi.org/10.1175/JAS3646.1.

——, 2008: Can a descending rain curtain in a supercell instigate tornadogenesis barotropically? *J. Atmos. Sci.*, **65**, 2469–2497, https://doi.org/10.1175/2007JAS2516.1.

——, 2015a: Formulas for parcel velocity and vorticity in a rotating Cartesian coordinate system. *J. Atmos. Sci.*, **72**, 3908–3922, https://doi.org/10.1175/JAS-D-15-0015.1.

——, 2015b: A review of supercell and tornado dynamics. *Atmos. Res.*, **158–159**, 274–291, https://doi.org/10.1016/j.atmosres.2014.04.007.

——, 2017: Roles of streamwise and transverse partial-vorticity components in steady inviscid isentropic supercell-like flows. *J. Atmos. Sci.*, **74**, 3021–3041, https://doi.org/10.1175/JAS-D-16-0332.1.

——, 2021: Invented forces in supercell models. *J. Atmos. Sci.*, **78**, 2927–2939, https://doi.org/10.1175/JAS-D-21-0082.1.

——, and H. E. Brooks, 1993: Mesocyclogenesis from a theoretical perspective. *The Tornado: Its Structure, Dynamics, Prediction, and Hazards*, *Geophys. Monogr.*, No. 79, Amer. Geophys. Union, 105–114.

——, and P. Markowski, 2013: Lifting of ambient air by density currents in sheared environments. *J. Atmos. Sci.*, **70**, 1204–1215, https://doi.org/10.1175/JAS-D-12-0149.1.

——, and ——, 2021: Circulation around a constrained curve: An alternative analysis tool for diagnosing the origins of tornado rotation in numerical supercell simulations. *J. Atmos. Sci.*, **78**, 2895–2909, https://doi.org/10.1175/JAS-D-21-0020.1.

——, D. W. Burgess, and M. Foster, 1990: Test of helicity as a tornado forecast parameter. Preprints, *16th Conf. on Severe Local Storms*, Kananaskis Provincial Park, AB, Canada, Amer. Meteor. Soc, 588–592.

——, R. J. Trapp, and H. B. Bluestein, 2001: Tornadoes and tornadic storms. *Severe Convective Storms*, *Meteor. Monogr.*, No. 50, Amer. Meteor. Soc., 167–222, https://doi.org/10.1175/0065-9401-28.50.167.

D'haeseleer, W. D., W. N. G. Hitchon, J. D. Callen, and J. L. Shohet, 1991: *Flux Coordinates and Magnetic Field Structure*. Springer-Verlag, 241 pp.

Droegemeier, K. K., S. M. Lazarus, and R. Davies-Jones, 1993: The influence of helicity on numerically simulated storms. *Mon. Wea. Rev.*, **121**, 2005–2029, https://doi.org/10.1175/1520-0493(1993)121<2005:TIOHON>2.0.CO;2.

Dutton, J. A., 1976: *The Ceaseless Wind*. McGraw-Hill, 579 pp.

Fujita, T. T., 1959: Detailed analysis of the Fargo tornadoes of June 20, 1957. U.S. Weather Bureau Tech. Rep. 5, 29 pp.

——, 1975: New evidence from April 3–4, 1974 tornadoes. Preprints, *Ninth Conf. on Severe Local Storms*, Norman, OK, Amer. Meteor. Soc., 248–255.

Kanehisa, H., 2002: A nonlinear extension of the helicity formula for convective storms. *J. Meteor. Soc. Japan*, **80**, 1301–1306, https://doi.org/10.2151/jmsj.80.1301.

Klemp, J. B., 1987: Dynamics of tornadic thunderstorms. *Annu. Rev. Fluid Mech.*, **19**, 369–402, https://doi.org/10.1146/annurev.fl.19.010187.002101.

——, and R. Rotunno, 1983: A study of the tornadic region within a supercell thunderstorm. *J. Atmos. Sci.*, **40**, 359–377, https://doi.org/10.1175/1520-0469(1983)040<0359:ASOTTR>2.0.CO;2.

Lamb, H., 1945: *Hydrodynamics*. Dover, 738 pp.

Lemon, L. R., and C. A. Doswell III, 1979: Severe thunderstorm evolution and mesocyclone structure as related to tornadogenesis. *Mon. Wea. Rev.*, **107**, 1184–1197, https://doi.org/10.1175/1520-0493(1979)107<1184:STEAMS>2.0.CO;2.

Lilly, D. K., 1982: The development and maintenance of rotation in convective storms. *Intense Atmospheric Vortices*, L. Bengtsson and J. Lighthill, Eds., Springer-Verlag, 149–160.

——, 1986: The structure, energetics and propagation of rotating convective storms. Part II: Helicity and storm stabilization. *J. Atmos. Sci.*, **43**, 126–140, https://doi.org/10.1175/1520-0469(1986)043<0126:TSEAPO>2.0.CO;2.

Margenau, H., and G. M. Murphy, 1956: *The Mathematics of Physics and Chemistry*. 2nd ed. Van Nostrand, 604 pp.

Markowski, P. M., and Y. P. Richardson, 2014: The influence of environmental low-level shear and cold pools on tornadogenesis: Insights from idealized simulations. *J. Atmos. Sci.*, **71**, 243–275, https://doi.org/10.1175/JAS-D-13-0159.1.

——, and G. Bryan, 2016: LES of laminar flow in the PBL: A potential problem for convective storm simulations. *Mon. Wea. Rev.*, **144**, 1841–1850, https://doi.org/10.1175/MWR-D-15-0439.1.

Miller, R. K., and A. N. Michel, 1982: *Ordinary Differential Equations*. Academic Press, 351 pp.

Mobbs, S. D., 1981: Some vorticity theorems and conservation laws for non-barotropic fluids. *J. Fluid Mech.*, **108**, 475–483, https://doi.org/10.1017/S002211208100222X.

Orf, L., 2019: A violently tornadic supercell thunderstorm simulation spanning a quarter-trillion grid volumes: Computational challenges, I/O framework, and visualizations of tornadogenesis. *Atmosphere*, **10**, 578, https://doi.org/10.3390/atmos10100578.

——, R. Wilhelmson, B. Lee, C. Finley, and A. Houston, 2017: Evolution of a long-track violent tornado within a simulated supercell. *Bull. Amer. Meteor. Soc.*, **98**, 45–68, https://doi.org/10.1175/BAMS-D-15-00073.1.

Roberts, B., M. Xue, and D. T. Dawson, 2020: The effect of surface drag strength on mesocyclone intensification and tornadogenesis in idealized supercell simulations. *J. Atmos. Sci.*, **77**, 1699–1721, https://doi.org/10.1175/JAS-D-19-0109.1.

Rotunno, R., 1981: On the evolution of thunderstorm rotation. *Mon. Wea. Rev.*, **109**, 577–586, https://doi.org/10.1175/1520-0493(1981)109<0577:OTEOTR>2.0.CO;2.

——, and J. B. Klemp, 1982: The influence of the shear-induced pressure gradient on thunderstorm motion. *Mon. Wea. Rev.*, **110**, 136–151, https://doi.org/10.1175/1520-0493(1982)110<0136:TIOTSI>2.0.CO;2.

——, and ——, 1985: On the rotation and propagation of simulated supercell thunderstorms. *J. Atmos. Sci.*, **42**, 271–292, https://doi.org/10.1175/1520-0469(1985)042<0271:OTRAPO>2.0.CO;2.

——, P. M. Markowski, and G. H. Bryan, 2017: "Near ground" vertical vorticity in supercell thunderstorm models. *J. Atmos. Sci.*, **74**, 1757–1766, https://doi.org/10.1175/JAS-D-16-0288.1.

Salmon, R., 1998: *Lectures on Geophysical Fluid Dynamics*. Oxford University Press, 378 pp.

Scorer, R. S., 1997: *Dynamics of Meteorology and Climate*. Praxis, 686 pp.

Shapiro, A. H., 1972: Vorticity. *Illustrated Experiments in Fluid Mechanics: The NCFMF Book of Film Notes*, MIT Press, 63–74, http://web.mit.edu/hml/ncfmf/09VOR.pdf.

Smith, R. K., and L. M. Leslie, 1979: A numerical study of tornadogenesis in a rotating thunderstorm. *Quart. J. Roy. Meteor. Soc.*, **105**, 107–127, https://doi.org/10.1002/qj.49710544308.

Trapp, R. J., and R. Davies-Jones, 1997: Tornadogenesis with and without a dynamic pipe effect. *J. Atmos. Sci.*, **54**, 113–133, https://doi.org/10.1175/1520-0469(1997)054<0113:TWAWAD>2.0.CO;2.

Wade, A. R., M. C. Coniglio, and C. L. Ziegler, 2018: Comparison of near- and far-field supercell inflow environments using radiosonde observations. *Mon. Wea. Rev.*, **146**, 2403–2415, https://doi.org/10.1175/MWR-D-17-0276.1.